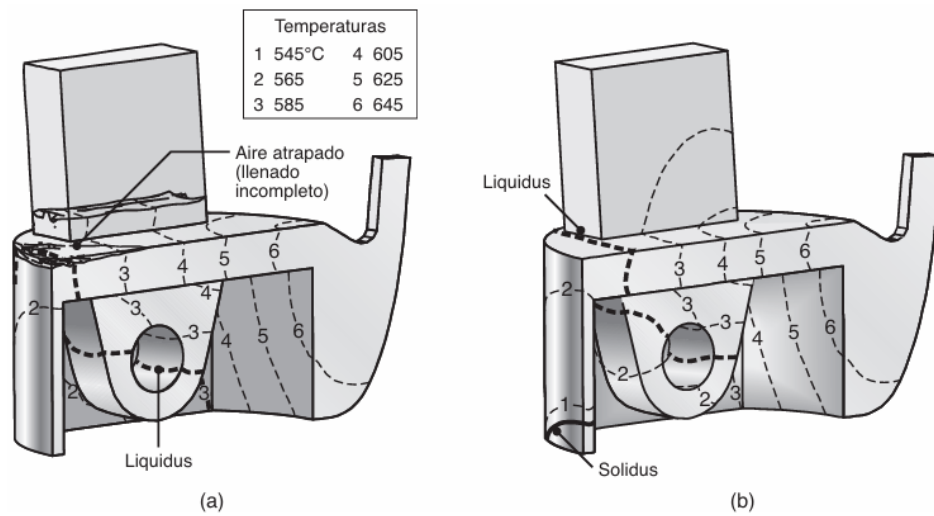
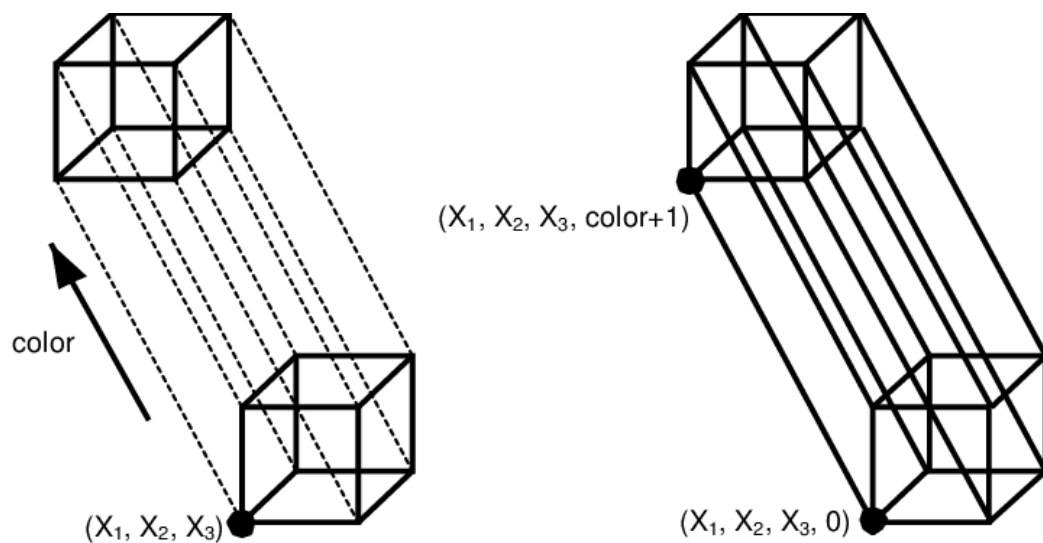


## Composites\_propellants(I)



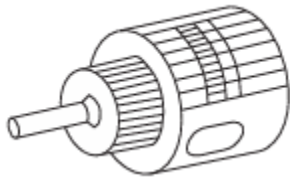
Composite structures Material and manufacturing process improvements, for composites in particular, generally increase specific strength and stiffness, while improved thermal stability for items such as optical benches is being achieved with carbon-carbon and ceramic materials. Carbon fibres derived from mesophase pitch give improved conductivity and modulus over standard carbon fibres derived from polyacrylonitrile (PAN), but they have lower compressive strength. This is good for optical benches but can be a problem at joints in highly loaded primary structures. Introducing carbon nanotubes into composite resins and adhesives or growing them onto the sides of carbon fibres improves thermal and electrical conductivity, strength and stiffness. Draping, weaving and stitching of fibres are being used to generate complex shapes which can be complemented by resin transfer moulding or a resin injection process. By integrating systems into composite structures, we may approach the concept of the intelligent structure. Already optical fibres can be embedded into a carbon fibre matrix allowing signals to pass along skins.



**Points:**

- mechanical including kapton and aluminium laminates,
- physical techniques including shape memory materials and solvent evaporation which suffers from out-gassing problems,
- chemical, thermal and/or UV curing,
- cas catalysed polymers.

For small spacecraft for low Earth orbit constellations or small-scale, single experiments, the designer is required not only to produce an efficient structure to maximize payload but also to respond to the ever-increasing commercial pressure of schedule and cost. Moulded, single component structures that can be stacked for multiple launches are an attractive proposition. The possibility of large numbers of spacecraft for the proposed global constellations.



The ACS designer will need to know the required time-history of the rotational motion, the angular rate  $\omega$  which is required of the spacecraft, and of any parts of it that can move independently on bearings. The angular momentum  $H_c$  and the torque  $T$  needed to produce it may then be calculated from the Newtonian law  $dH_c/dt = T$  where  $H_c$  is the angular momentum referred to the centre-of-mass  $C$ , detailed in equations.

**EXTERNAL TORQUES**

*Source:*

*Aerodynamic*

*Magnetic*

*Gravity gradient*

*Solar radiation*

*Thrust misalignment*

**INTERNAL TORQUES**

*Source:*

*Mechanisms*

*Fuel movement*

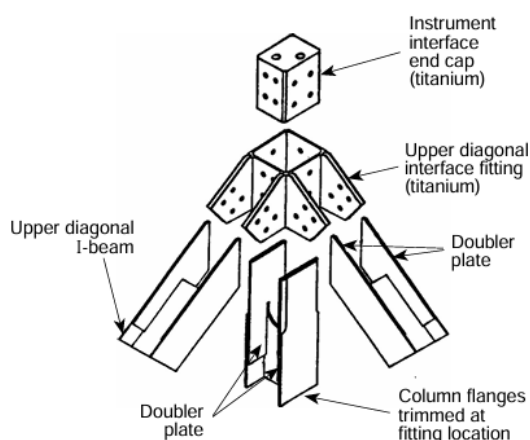
*Astronaut movement*

*Flexible appendages*  
*General mass movement*

**HEIGHT RANGE OVER WHICH IT IS POTENTIALLY DOMINANT**

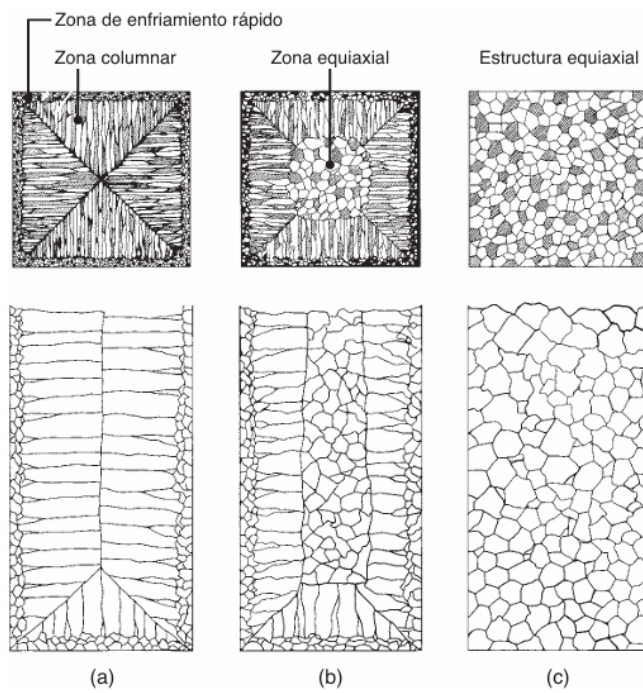
*Aerodynamic: <about 500km*  
*Magnetic: 500–35000km*  
*Gravity gradient: 500–35000km*  
*Solar radiation: >700km*  
*Thrust misalignment: all heights*

Propellants are often tailored to and classified by specific applications, such as space launch booster propellants or tactical missile propellants, each having specific chemical ingredients, different burning rates, different physical properties, and different performance. Table 12–1 shows four rocket motor applications (each with somewhat different propellants), plus several gas generator applications and an artillery shell application. Propellants for rocket motors produce hot (over 2400 K) gases and are used for thrust, but gas generator propellants operate with lower-temperature combustion gases (800 to 1200 K in order to use uncooled hardware) and are used to produce power, not thrust. 2. Double-base (DB)\* propellants form a homogeneous propellant grain, usually a nitrocellulose (NC)\*—a solid ingredient that absorbs liquid nitroglycerine (NG), plus minor percentages of additives. The major ingredients are highly energetic materials and they contain both fuel and oxidizer. Both extruded double-base (EDB) and cast double-base (CDB) propellants have found extensive applications, mostly in small tactical missiles of older design. By adding crystalline nitramines (HMX or RDX)\* Both performance and density can be improved; these are sometimes called cast-modified double-base propellants. Adding an elastomeric binder (rubber-like, such as crosslinked polybutadiene) further improves the physical properties and allows more nitramine and thus increasing performance slightly. The resulting propellant is called elastomeric-modified cast double-base (EMCDB). These four classes of double-base propellants have nearly smokeless exhausts. Adding some solid ammonium perchlorate (AP) and aluminum (Al) increases the density and the specific impulse slightly, but exhaust gases become smoky—such propellant is called composite-modified double-base propellant or CMDB.

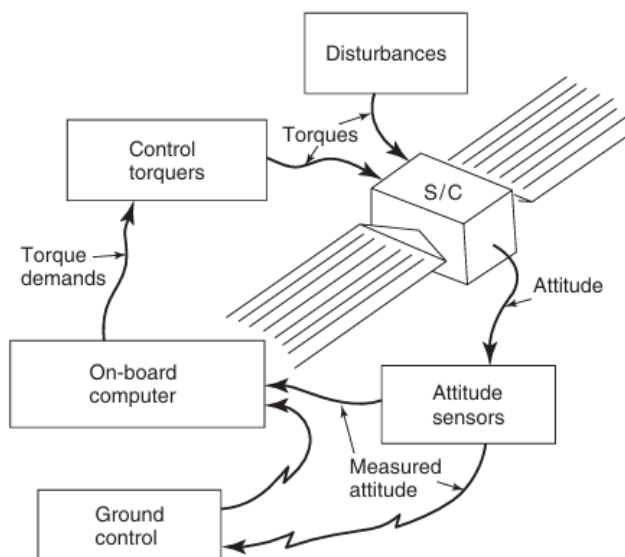




The Dynamics: The dynamic equations for this spacecraft, treated as a rigid body, are covered in Section 3.4.1 of Chapter 3, using principal axes for the analysis. With small angular velocities the responses about these axes are largely uncoupled and may be approximated by  $I_{xx} \cdot \omega_x = T_x$ ,  $I_{yy} \cdot \omega_y = T_y$ ,  $I_{zz} \cdot \omega_z = T_z$



Composite propellants form a heterogeneous propellant grain between oxidizer crystals and powdered fuel (usually aluminum) held together in a matrix of synthetic rubber (or plastic) binder, such as polybutadiene (HTPB).<sup>\*</sup> Composite propellants are cast from a mix of solid (AP crystals, Al powder) and liquid (HTPB, PPG)<sup>\*</sup> ingredients. The propellant is hardened by crosslinking or curing the liquid binder polymer with a small amount of curing agent, and curing it in an oven, where it becomes solid. In the past four decades composites have been the most commonly used class of propellant.



Flights at high speeds (Supersonic aerodynamics)

The speed of sound or sonic velocity is the speed of propagation when the air changes Its pressure or the particles in the air flow change their pressure level and speed when they collide with a wing. The speed of propagation is very fast and it is not about flying faster than sound, but about the speed of propagation in the air and the fact that the pressure is disturbed. There is disturbance of the pressure effect when flying at high speeds.

The speed of an object compared to the speed of sound, or the speed at which small pulses of pressure are transmitted in the airflow around the aircraft wing, is important to parameterize, or write a parameter of, the supersonic airflow.

**Variables:** Given the important variables or indices of the speed of sound, adiabatic coefficient, constants and Temperature:

- “a” is the speed of sound.
- “ $\gamma$ ” is the adiabatic coefficient (for air,  $\gamma=1.4$ )
- “R” is the ideal gas constant (for air,  $R=287 \text{ J/(kg}\cdot\text{K)}$ ) “ $R=287\text{J/(kg}\cdot\text{K)}$ ”
- “T” is the absolute temperature in Kelvin.

Height	Temperature	speed of sound	MPH Kts
--------	-------------	----------------	---------

```
% Parameters
gamma = 1.4; % Adiabatic coefficient for air
R = 287; % Ideal gas constant for air in J/(kg·K)
T = 300; % Temperature in Kelvin (example: 300K)

% Calculate the speed of sound
a = sqrt(gamma * R * T);

% Show the result
fprintf('The speed of sound is %.2f m/s\n', a);
```

a = squareRoot % R T

#### Code Explanation

1. **Parameter Definition:** The values of  $\gamma$ , R and T are defined. In this example, T has been set to 300 K, which is a typical temperature for air at sea level.
2. **Calculation of the Speed of Sound:** The formula  $a=\sqrt{\gamma RT}$  is used to calculate the speed of sound.

3. **Show the result:** The result is printed using `fprintf`.

### Aircraft flaps in approximate calculations:

Stall speed with flaps fully extended and retracted is calculated and displayed, and will also plot the relationship between lift coefficient and stall speed. You can run this code in a Python environment to get the results and visualization. On the other hand, variables are a way to synthesize calculations with programming languages and processes at an automatic or automated level of variables where the aerodynamic variables are:

1. W is the weight of the aircraft.
2. Weigh the density of the air.
3. V<sub>stall</sub> is the stall speed.
4. S is the reference area.

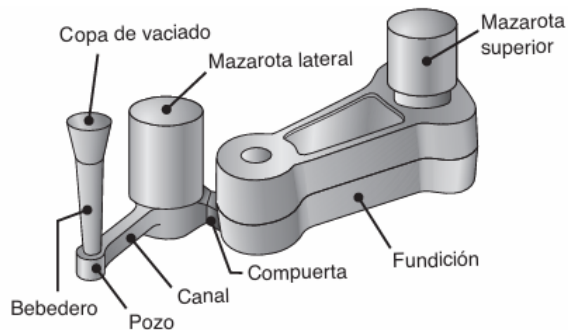


**FIGURA 10.8** Esquema de una fundición característica con mazarotas y compuertas. Las mazarotas sirven como contenedores que suministran metal fundido a la fundición conforme se contrae durante la solidificación.

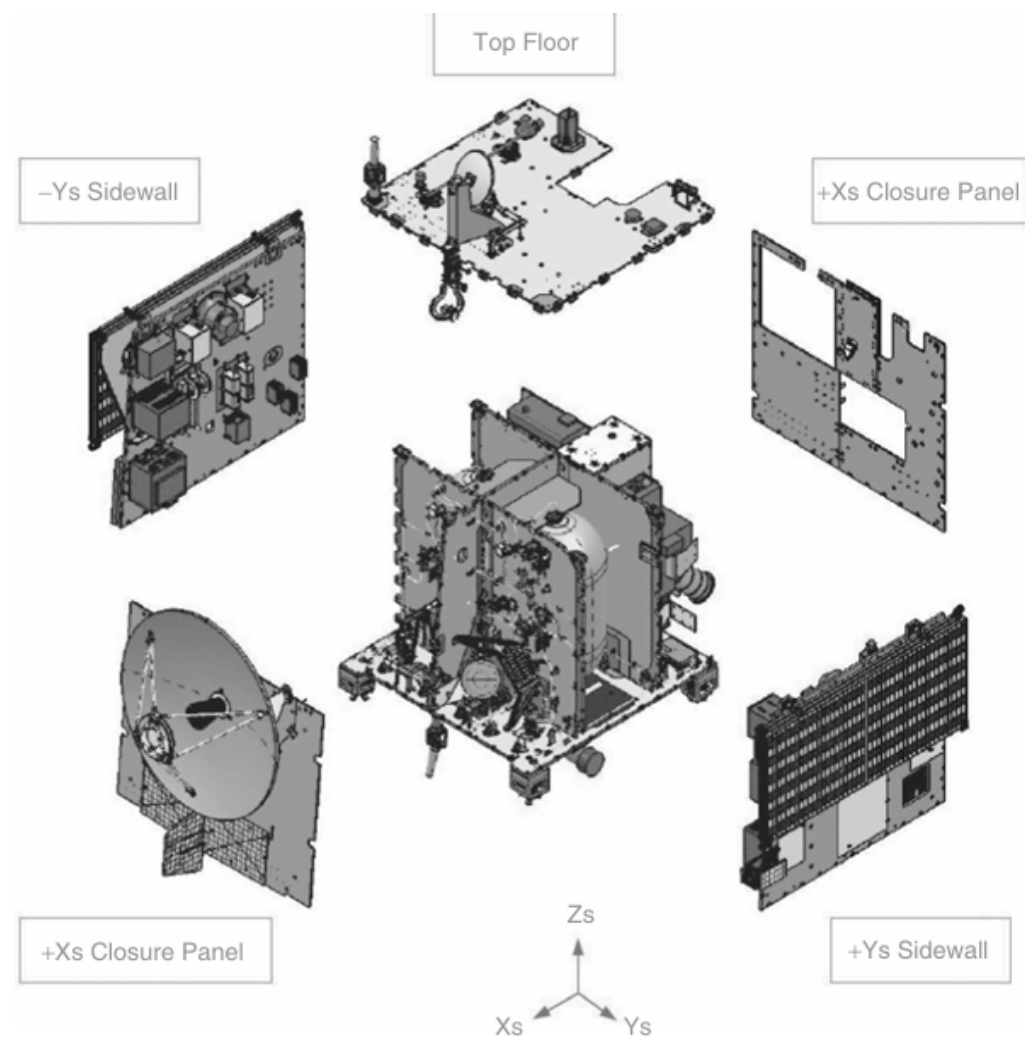


**Figure 8.25** Mars Express structure configuration. (Reproduced by permission of EADS Astrium Ltd.)

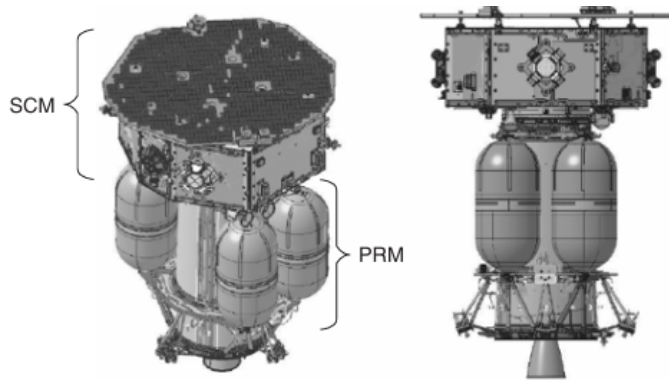
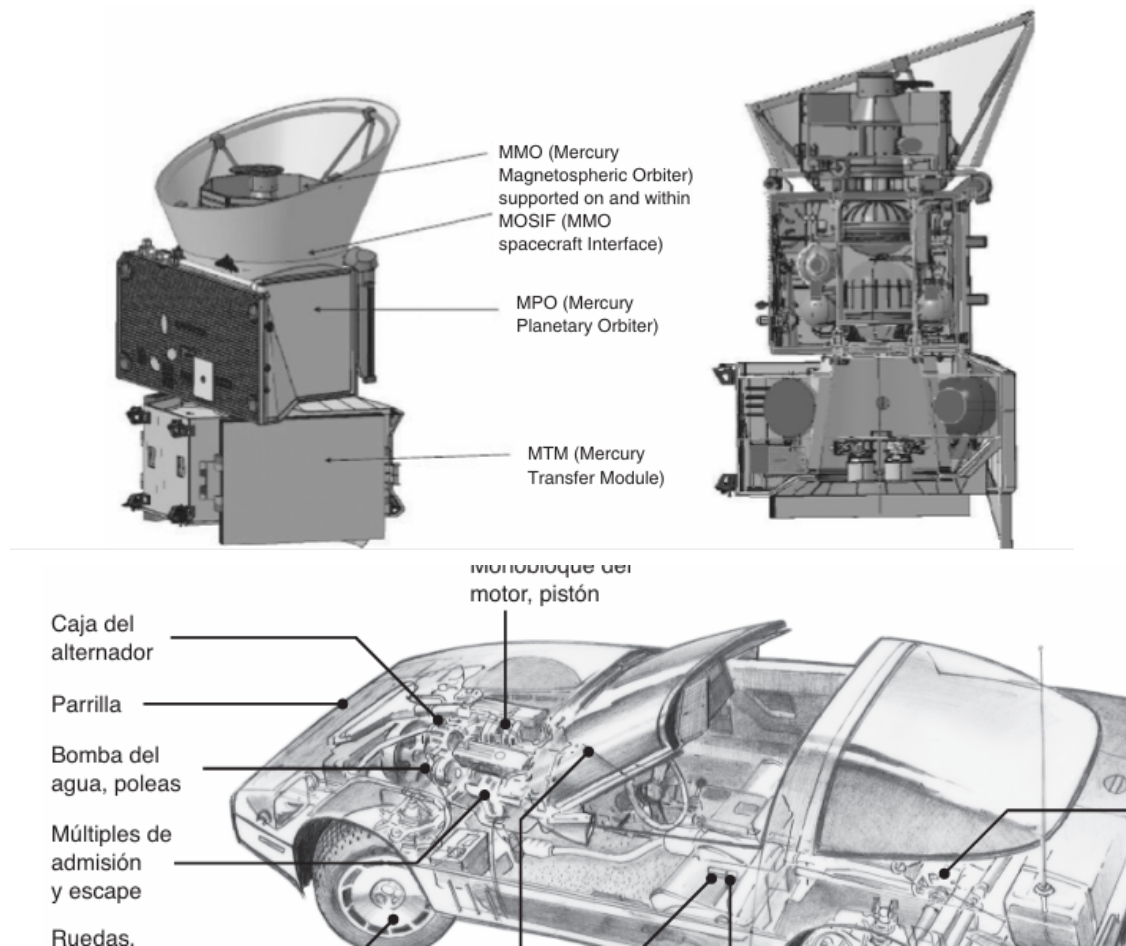
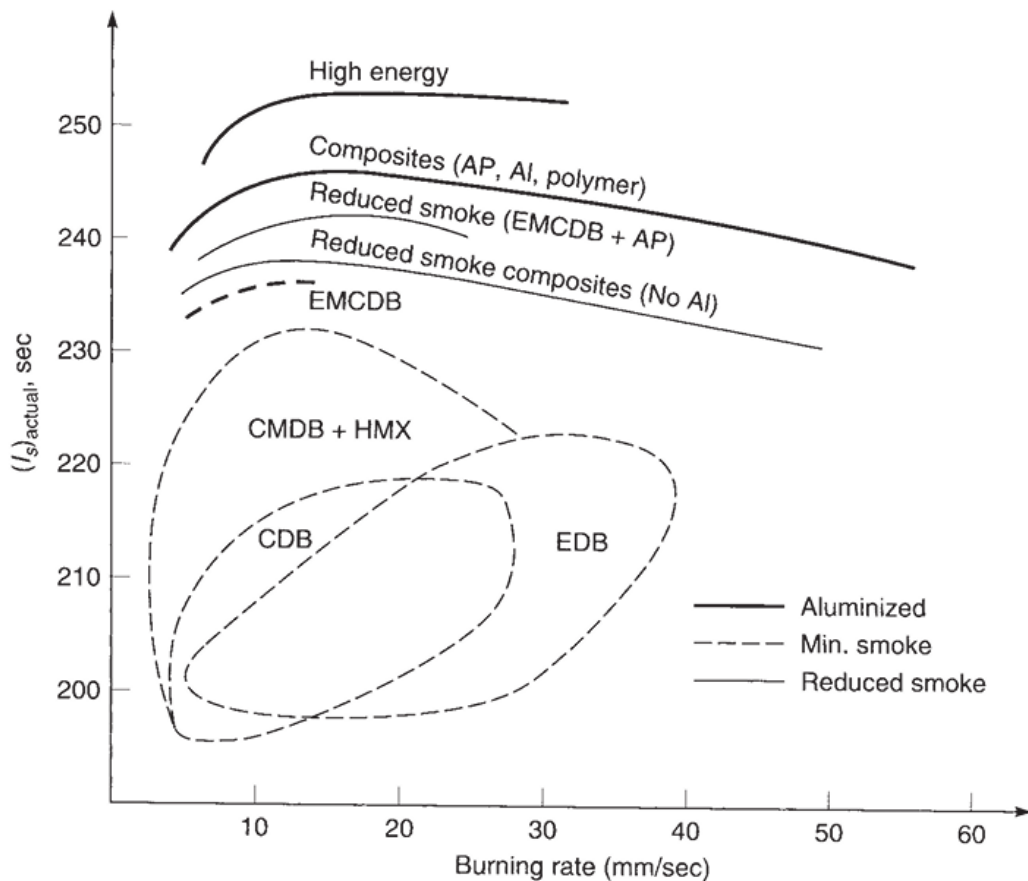


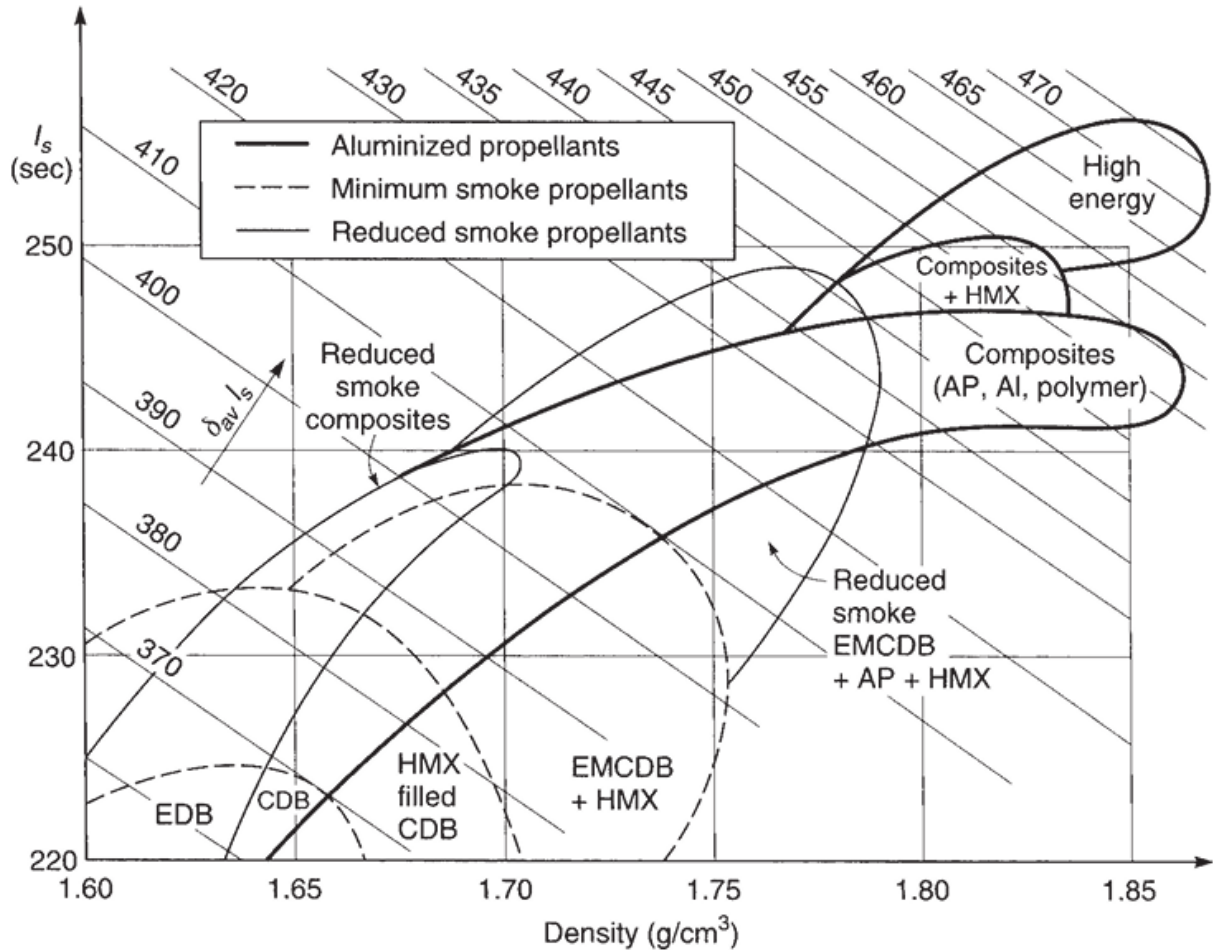
**Figure 8.21** Lisa Pathfinder Propulsion Module. (Reproduced by permission of EADS Astrium Ltd.)



Modified composite propellant where an energetic nitramine (HMX or RDX) is added for obtaining some added performance and also a somewhat higher density. c. Modified composite propellant where an energetic plasticizer such as nitroglycerine (used in double-base propellants) is added to give increased performance. Sometimes HMX is also added. d. High-energy composite solid propellant (with added aluminum), where the organic elastomeric binder and the plasticizer are largely replaced by highly

energetic materials and where some of the AP is replaced by HMX and RDX. Hexanitrohexaazaiso-wurtzitane or CL-20 is a recent propellant ingredient being used; it is produced outside of the United States. Lower-energy composite propellant, where ammonium nitrate (AN) is the crystalline oxidizer (not AP). These are used for gas generator propellants. When large amounts of HMX are added, they become minimum smoke propellants with fair performance. Propellants may also be classified by the smoke density in the exhaust plume as smoky, reduced smoke, or minimum smoke (essentially smokeless). Aluminum powder, a desirable fuel ingredient for performance, is oxidized to aluminum oxide during burning, which yields visible, small, solid smoky particles in the exhaust gas. Most composite propellants (e.g., AP) are also smoky. By replacing APP with HMX and RDX and by using energetic binders and plasticizers to compensate for eliminating aluminum, the amount of smoke may be considerably reduced in composite propellants. Carbon (soot) particles and metal oxides, such as zirconium oxide or iron oxide, are also visible in high enough concentrations.





**Compressible Flow:** At high speeds, the compressibility of air becomes significant, affecting the density and pressure of the flow around the object.

**Mach number:** It is the relationship between the speed of the object and the speed of sound in the medium. It is used to classify flight regimes: subsonic ( $\text{Mach} < 1$ ), transonic ( $\text{Mach} \approx 1$ ), supersonic ( $\text{Mach} > 1$ ), and hypersonic ( $\text{Mach} > 5$ ).

**Shock Waves:** They are discontinuities in the flow that occur when the object exceeds the speed of sound, resulting in abrupt changes in pressure, temperature and density of the air.

**Prandtl-Glauert effect:** Describes the intensification of pressure on the surface of the object as it approaches the speed of sound, creating an increase in aerodynamic drag.

**Modified Bernoulli's Law:** At high speeds, Bernoulli's law is adjusted to account for the compressibility of the flow, allowing analysis of the pressure distribution in the moving object.

**Wave Drag:** A component of aerodynamic drag that becomes significant at transonic and supersonic speeds, caused by the formation of shock waves.

**Conclusion:** These basic principles are fundamental to design and analyze aircraft and other objects that operate at high speeds, ensuring efficiency and stability in extreme conditions.

**Fluids:** Since air is a fluid and air is also the object of study of aerodynamics,

It is convenient to establish some basic properties of fluids. Fluid is a body whose molecular arrangement is such that small forces are enough to change the relative position of these moving particles. Liquids and gases are fluids and demonstrate their molecular property of fluids by changing shape easily. "Fluids change their molecular shape, the structures of their particles"

**Steady regime or laminar flow:** It is one in which at any point in the fluid, the velocity vector remains constant. This means that at any point in the fluid, the particles that pass through that point have the same speed, direction and direction.

Example: To calculate the maximum clean lift coefficient;

- W is the weight of the aircraft.
- P is the density of air.
- (V)<sub>stall</sub> is the stall speed.
- S is the reference area.

**Software to do flap calculations:**

```
import numpy as np
import matplotlib.pyplot as plt

# Data provided
W_max = 12500 # Maximum allowable takeoff weight in kg
fuel_consumed = 1200 # Fuel consumed in kg
rho = 1.225 # Air density in kg/m^3
S = 28.15 # Reference area in m^2
g = 9.81 # Acceleration due to gravity in m/s^2
CL_max_extended_flaps = 1.90 # Maximum lift coefficient with fully
extended flaps
CL_max_flaps_refolded = 0.5 # Maximum lift coefficient
```

## *Types of aircraft wing profiles (definitions)*

**1.Wing chord:** It is a straight line that joins the forward end of an aircraft wing or leading edge to the trailing edge or trailing edge.

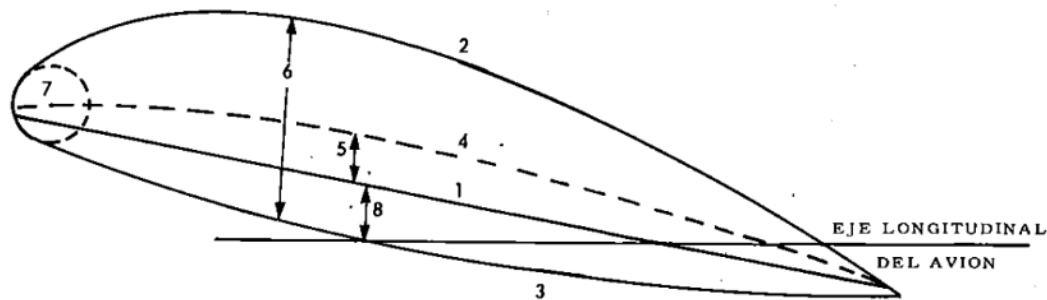
**2.Upper curvature:** Curvature of a semicircle that joins the forward leading edge of the wing and the rear end on the straight line of flight.

**3.Bottom curvature:** Continuation of the line of the upper curvature below the chord.

**6.Maximum thickness:** Maximum distance between the upper and lower curvatures.

**7.Leading edge radius:** Radius of curvature or a geometric circle

**8.Angle of incidence:** Angle formed by the middle chord and the length or longitudinal axis of an aircraft.



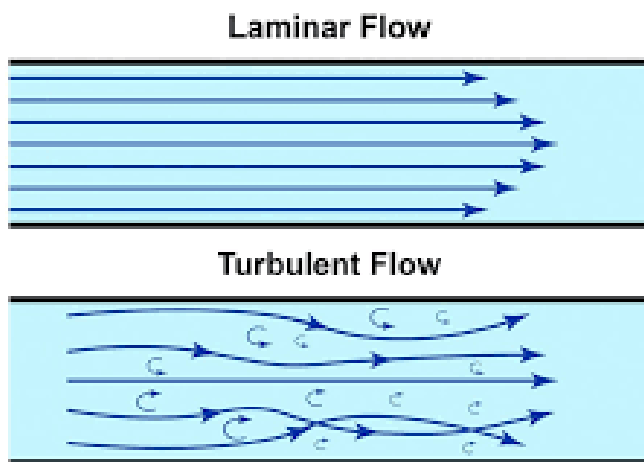
**Relations with tensors:** By relating high-speed aerodynamics to the theory of relativity and tensors in the context of a black hole, we can consider how airflow and Bernoulli's principles would be modified in a curved spacetime. General relativity tells us that the presence of a black hole curves space-time, and this effect can alter the behavior of airflow and lift in a hypothetical aircraft moving near the black hole.

**Propellant:** Composite propellants are shown to have a wide range of burning rates and densities; most of them have specific gravities between 1.75 and 1.81 and burning rates between 7 and 20 mm/sec.

Composite propellants give higher densities, specific impulse, and a wider range of burning rates than others. DB propellants and AN propellants have lower performance and density. Most composite propellants display similar performance and density but with a wider range of burning rates. The highest performance indicated is for a CMDB propellant whose ingredients are identified as DB/AP-HMX/AI

Propellant selection is critical to rocket motor design. Desirable propellant characteristics are listed below and further discussed in other parts of this book. Many requirements for particular solid propellant rocket motors will influence priorities for choosing these characteristics:

1. High performance means Specific Impulse; this implies a high gas temperature and/or low exhaust gas molecular mass.
2. Predictable, reproducible, and initially adjustable burning rate to fit grain design needs and thrust-time requirements.
3. For minimum variations in thrust or chamber pressure during burning, both the pressure or burning rate exponent and the temperature coefficient should be small.



#### Parameter Definition:

- **V** is the speed of the aircraft, which in this case is approximately the speed of sound.
- **a** is the speed of sound.
- **mach\_number** calculates the Mach number of the aircraft.

#### Pressure Distribution:

- **x** and **and** They define the grid on which the pressure distribution will be calculated.
- **pressure** is a simplification of the pressure distribution around the wing.

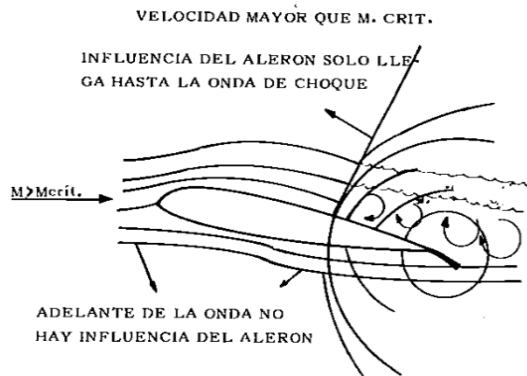
#### Shock Wave Effect:

- `shock_wave` simulates a shock wave at the edge of the wing.

**Display:**

- It is used `contourf` to create a filled contour map of the pressure distribution and shock waves.
- `plt.axhline` and `plt.axvline` They add lines to highlight the position of the wing and the shock wave.
- `plt.legend` adds a legend for the shock wave.

1. Problems with transonic flights include decreased aerodynamic characteristics of the wing (increased drag and decreased lift)
2. Pounding
3. Loss of effectiveness of flight controls and instability
4. Sonic barrier problems.
5. The pressure waves transmitted by the deflection of the aileron: The variables are the highest speed,  $M > M_{crit}$ , the influence wave and the shock wave.



**Shock waves and superluminal pulsars in theories about black holes:**

The vibrations or hums that the pilot perceives in the control stick are an indication to let him slow down. The pilot has a prior warning that announces the knocking and vibrations that are produced by aircraft turbulence. Particles of a different quantum type than the one known do not consist of a defined mass and it is possible that their dimensions consist of a property of transposition (D) at very high speeds and that a possible aircraft could be composed of superluminal quantum particles (tachyons), or qubits (Aircraft) or something similar, comparing this concept or idea with the curvature of tensors of Riemann black holes and the theory of Cherenkov Radiation, new patterns could be established within the framework of theoretical physics for black holes. But here it is necessary to carry out an analysis of the structure of frequencies, tensors and Cherenkov radiation.

## PROPELLANT TYPE ANALYSIS

### DOUBLE BASE (EXTRUDED)

Advantages:

- Modest cost.
- Nontoxic clean exhaust, smokeless.
- Good burn rate control.
- Wide range of burn rates.
- Simple well-known manufacturing process.
- Good mechanical properties.
- Low-temperature coefficient.
- Very low pressure exponent.
- Plateau burning is possible.

Disadvantages:

- Freestanding grain requires structural support.
- Low performance and low density.
- High to intermediate hazard in manufacture.
- Potential storage issues with NG bleeding out.
- Diameter limited by available extrusion presses.
- Classified as 1.1a.

### DOUBLE BASE (CASTABLE)

Advantages:

- Wide range of burn rates.
- Nontoxic smokeless exhaust.
- Relatively safe to handle.
- Simple, well-known process.
- Modest cost.
- Good mechanical properties.
- Good burn rate control.
- Low-temperature coefficient.
- Plateau burning can be achieved.

Disadvantages:

- NG may bleed out or migrate.
- High to intermediate manufacturing hazard.
- Low performance and low density.
- Higher cost than extruded double base.
- Classified as 1.1a.

### COMPOSITE MODIFIED DOUBLE BASE (CMDB) WITH SOME AP AND Al

Advantages:

- Higher performance.

- Good mechanical properties.
- High density.
- Less likely to have combustion stability problems.
- Intermediate cost.
- Good background experience.

Disadvantages:

- Complex facilities required for manufacturing.
- Some smoke in exhaust.
- High flame temperature.
- Moisture-sensitive.
- Moderately toxic exhaust.
- Hazards in manufacturing.
- Modest ambient temperature range.
- High value of pressure exponent (0.8–0.9).
- Moderately high temperature coefficient.

#### COMPOSITE AP, Al, AND PBAN OR PU OR CTPB BINDER

Advantages:

- Reliable performance.
- High density.
- Long experience background.
- Modest cost.
- Good aging properties.
- Long cure time.
- Good overall performance.
- Usually stable combustion.
- Low to medium cost.
- Wide operational temperature range.
- Low to moderate temperature sensitivity.
- Good burn rate control.
- Usually good physical properties.
- Classified as 1.3.

Disadvantages:

- Modest ambient temperature range.
- High viscosity limits at maximum solid loading.
- High flame temperature.
- Toxic, smoky exhaust.
- Some formulations are moisture sensitive.
- Some burn-rate modifiers (e.g., aziridines) are carcinogens.

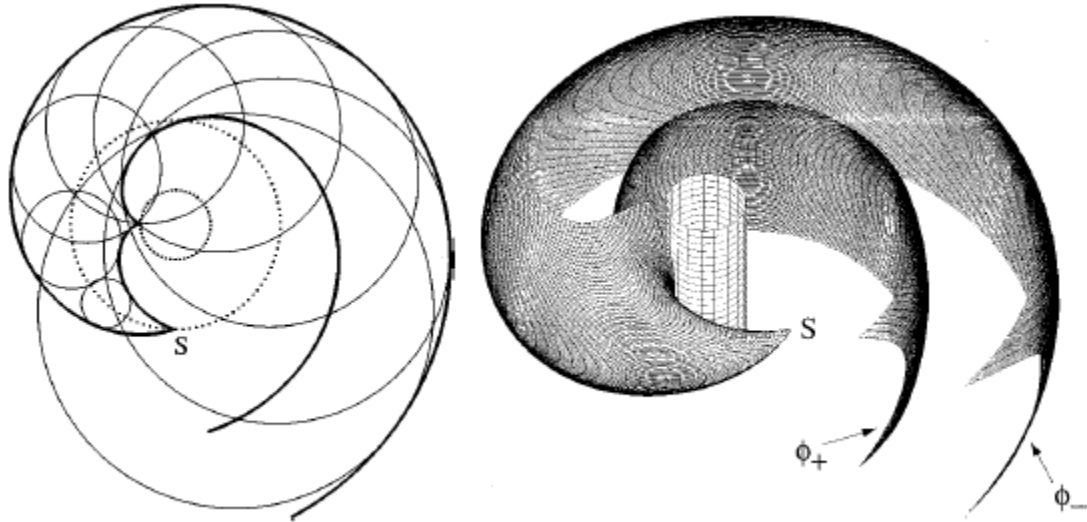
## COMPOSITE AP, Al, AND HTPB BINDER (MOST COMMON COMPOSITE PROPELLANT)

Advantages:

- Slightly better solid loading percentage and performance compared to PBAN or CTPB.
- Wide ambient temperature limits.
- Good burn-rate control.
- Usually stable combustion.
- Medium cost.
- Good storage stability.
- Wide range of burn rates.
- Good physical properties.
- Good experience background.
- Classified as 1.3.

Disadvantages:

- Complex facilities required for manufacturing.
- Moisture sensitive.
- Fairly high flame temperature.
- Toxic, smoky exhaust.



**Test Method Selection** Although the basic physics of test methods for composite materials are similar to those for testing metals or plastics, the heterogeneity, orthotropic, moisture sensitivity, and low ductility of typical composites often lead to major differences in test requirements, particularly for mechanical tests. These differences include:

- (1) The strong influence of constituent content on material response necessitates measurements of the material response of every specimen.
- (2) Properties should be evaluated in multiple directions.
- (3) Specimens should be conditioned to quantify and control moisture absorption and adsorption.
- (4) The methods of specimen alignment and load induction have increased importance for composites.
- (5) The consistency of failure modes requires some assumptions to be made.

**Glass Fibers** Glass fibers are usually drawn from a molten mixture of quartz sand, limestone, dolomite and paraffin, as well as a certain fraction of soda and boric acid [4]. To facilitate the process or to achieve the desired performance, an appropriate fraction of TiO<sub>2</sub>, ZrO<sub>2</sub> or Al<sub>2</sub>O<sub>3</sub> is also incorporated. The components and the drawing process greatly affect the performance of the final fibers. Glass fibers are non-combustible and do not decompose, and they are characterized by good chemical stability, good heat resistance, high tensile strength, high electrical insulation, low tensile strain, low insulation and a low coefficient of thermal expansion. They were the first fibers to be used for the preparation of polymer matrix composites. They are commonly known to be low-cost reinforcements for fiberglass-reinforced plastics (FRP) [5]. The diameters of the glass fibers vary from 5 to 20 lm, and a finer fiber diameter generally results in better performance. The types and specifications of commercially available glass fibers are mainly as follows: A-glass fiber, containing high alkali metal oxides; C-glass fiber, resistant to chemical attack; D-glass fiber, with a high dielectric property; E-glass fiber, with high electric insulation; M-glass fiber, with a high Young's modulus; S-glass fiber, with a high tensile strength; AR-glass fiber, alkaline resistant and suitable for reinforcing cement matrix composites.

## TYPES AND COMPOSITIONS OF COMMERCIAL GLASS FIBERS

### TYPE A:

- Primary Composition: High percentage of SiO<sub>2</sub>.
- Additional Elements: B<sub>2</sub>O<sub>3</sub>, CaO, Na<sub>2</sub>O, MgO.
- Notable Properties: Standard glass fiber composition with moderate mechanical stability.

### TYPE C:

- Primary Composition: Lower SiO<sub>2</sub> content compared to Type A.
- Additional Elements: Al<sub>2</sub>O<sub>3</sub>, B<sub>2</sub>O<sub>3</sub>, CaO, MgO.
- Notable Properties: Increased chemical resistance compared to traditional glass fibers.

### TYPE E:

- Primary Composition: Lower SiO<sub>2</sub> concentration.
- Additional Elements: B<sub>2</sub>O<sub>3</sub>, Al<sub>2</sub>O<sub>3</sub>, CaO.
- Notable Properties: Electrical insulation applications, good mechanical properties.

### TYPE E-CR:

- Primary Composition: Moderate SiO<sub>2</sub> content.
- Additional Elements: Al<sub>2</sub>O<sub>3</sub>, CaO, MgO, TiO<sub>2</sub>.
- Notable Properties: Corrosion-resistant formulation with better durability.

### TYPE M:

- Primary Composition: SiO<sub>2</sub> with additional stabilizers.
- Additional Elements: SO<sub>3</sub>, Li<sub>2</sub>O, ZnO, TiO<sub>2</sub>.
- Notable Properties: Enhanced thermal stability and resistance to environmental degradation.

### TYPE S:

- Primary Composition: High SiO<sub>2</sub> content.

- Additional Elements: High  $\text{Al}_2\text{O}_3$  percentage.
- Notable Properties: Superior mechanical strength, used in aerospace applications.

TYPE ZORAR:

- Primary Composition: High  $\text{SiO}_2$  concentration.
- Additional Elements:  $\text{ZrO}_2$ ,  $\text{TiO}_2$ .
- Notable Properties: Improved resistance to extreme thermal conditions and structural stability.

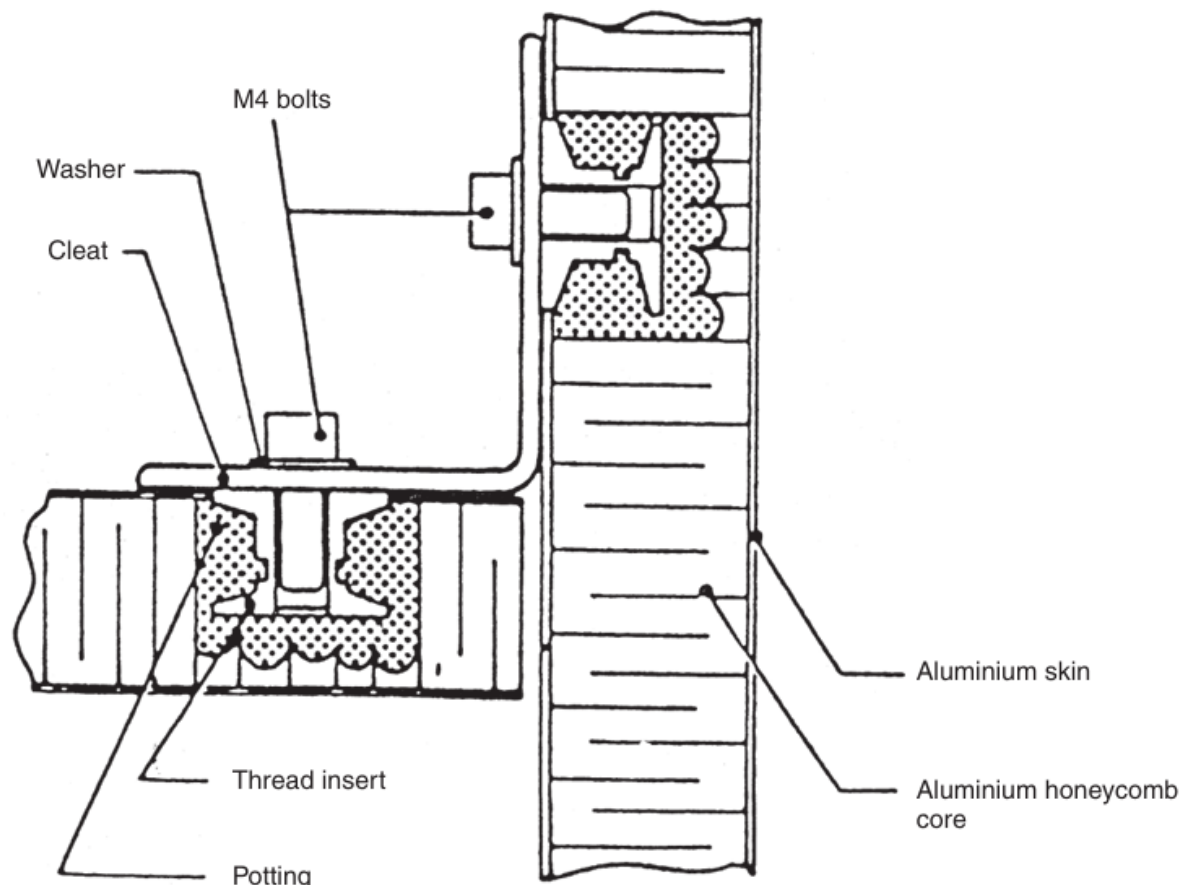


**Figure 8.7** Inserts and panel cleat joints. (Reproduced by permission of EADS Astrium Ltd.)

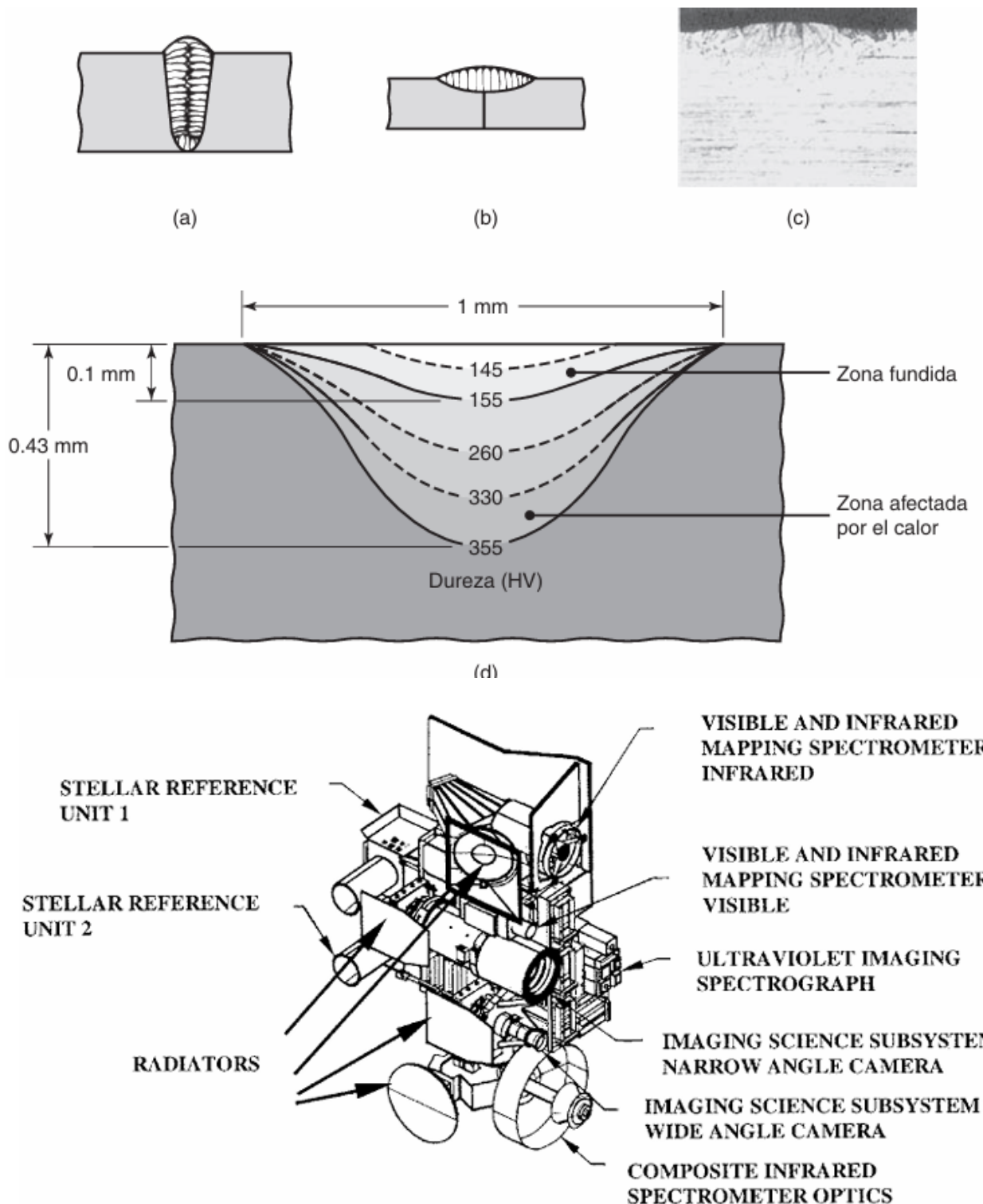


Figure 5. Remote Sensing Pallet with Instruments.

**E-Glass Fibers** E-glass fibers, also referred to as non-alkali glass fibers, were the first fiber species used for electronic insulation belts. They are a kind of Ca–Al–B–Si glass fiber with a total alkali content less than 0.8 wt%, which ensures their excellent corrosion resistance and high conductivity resistance. As a favored insulation material, they have been processed into electromagnetic wires, impregnation materials, mica products, laminated products and polymer matrix composite products. The insulation grade of these products varies from B, F and H to C, which enables their widespread use in the electric and electronic fields. They are also the most common fiber reinforcements for polymer matrix composites. They are regarded as ideal polymer strengthening glass fibers with a high strength, high Young's modulus, low density and good water resistance. As an example, they have accounted for 90% of the glass fiber market. They can be used both structurally and functionally. For example, E-glass fiber-reinforced rubber products or filter products can be used in the cement, power, metallurgy and carbon black industries where processing temperatures reach up to 150–300 °C. However, a significant disadvantage of E-glass fibers is their limited chemical corrosion resistance to acid or alkali media, thus restricting their application in a cement matrix.

## **Curvature and Dynamics of Black Holes**

### Introduction to General Relativity

The theory of general relativity, proposed by Albert Einstein in 1915, revolutionized our understanding of space, time and gravity. Unlike Newton's theory of gravitation, which describes gravity as a force acting at a distance, general relativity interprets gravity as a manifestation of the curvature of space-time. This curvature is caused by the presence of mass and energy.

### *What is a Tensor?*

To understand general relativity, it is essential to become familiar with tensors, which are fundamental mathematical tools in this theory. A tensor generalizes the concepts of scalars and vectors to higher dimensions and is used to describe the physical properties of a system at any point in spacetime.

**Scalar (Rank Tensor 0):** A quantity that does not change under coordinate transformations, such as the temperature at a point.

**Vector (Rank Tensor 1):** A quantity with magnitude and direction, such as speed.

**Rank 2 Tensor:** A matrix that can describe more complex properties, such as stresses in a material or space-time metrics.

In MATLAB, we can illustrate tensors using multidimensional matrices and arrays. For example, a rank 2 tensor can be represented as a matrix

```
% Example of a rank 2 tensor (a 3x3 matrix)
tensor_rango2 = [1, 2, 3; 4, 5, 6; 7, 8, 9];
disp('Rank Tensor 2:');
disp(tensor_rango2);
```

## *Space-Time and Metrics*

In general relativity, space and time are combined into a single entity called spacetime. The metric is a tensor that describes how distances and time intervals are measured in this curved spacetime. The metric tensor  $g_{\mu\nu}$  provides a way to calculate the separation between two events in spacetime.

## *Introduction to Riemann Geometry and Tensors*

### **Definition of Tensors**

A tensor is a mathematical object that generalizes the concepts of scalars, vectors and matrices. In the context of general relativity, tensors are fundamental to describing the properties of spacetime.

A rank 2 tensor in a 4-dimensional space (such as spacetime) can be represented as a 4x4 matrix.

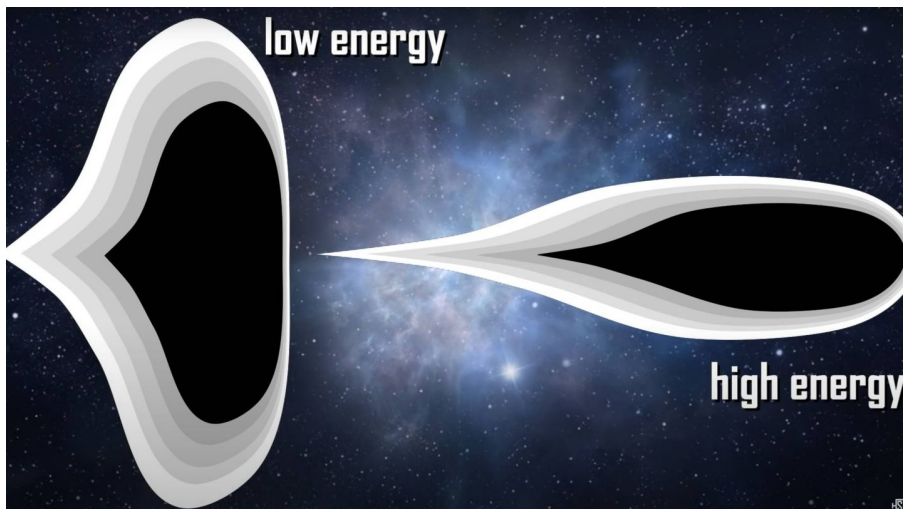
### Scalars, points and vectors

In what follows we restrict our attention to the real numbers  $\mathbb{R}$  and the ordinary geometric space  $E^3$ , an affine space of dimension 3 and endowed with the Euclidean metric.

The elements  $a \in \mathbb{R}$  are called scalars and can be considered as zeroth order tensors. The elements  $A \in E^3$  are called points. The coefficients  $(v_1, v_2, v_3)$  are called coordinates of  $v$  in the base  $(e_1, e_2, e_3)$ . A linear map  $T$  is called a tensor of order two on a vector space  $V: V \rightarrow V$ , so that

$\text{In } E^3 \ v \mapsto T v \in V$ .

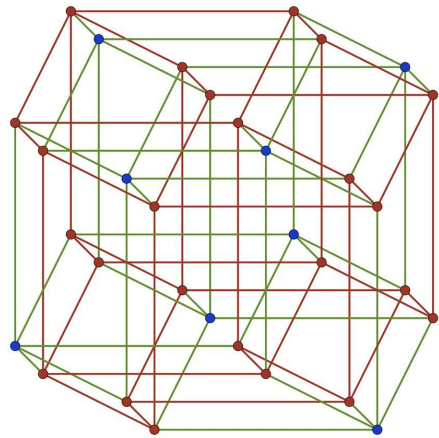
AR-Glass Fibers AR-glass fibers, namely alkali-resistant glass fibers, contain about 16 wt% ZrO<sub>2</sub>. They are used as reinforcements for cement matrix composites with an anti-alkaline property better than that of ordinary glass fibers. Compared with unreinforced cement, AR-glass fiber-reinforced cement has a 2–3 times higher tensile strength, a 3–4 times higher bending strength and a 15–20 times higher toughness. The reinforced composite can be used for manufacturing large panels, roof slabs, corrugated tiles, balcony slabs, all kinds of pipes and permanent templates.





Components: S-glass fibers can be made into a variety of twistless rovings, twist yarns, cloths and other products. If the coupling agent KH-550 is applied, they can be impregnated directly into epoxy, phenolic resins and nylon, and they act as reinforcements of polymer matrix composites that require high strength. The reinforced composites can be fabricated as weapon components such as rocket engine shells and launcher shells, plane spiral lamina and landing gear, radomes, artillery covers and fuses, deep water mine shells, bulletproof vests, and ammunition boxes. They have played an important role in improving arms performance. In civilian fields, they have been used in high-pressure containers such as air cylinders, health cylinders, lifeboats, refrigerated vessels and spiral laminas.

## Tensor Curvature



**Theory:** Tensors, aerodynamics and shock waves are useful to represent physical phenomena of Riemann curvature and represent parameters that help us build and search for new theories about curved spaces that are represented beyond three dimensions and make a comparative, that is, defining the laminar layer of an airplane with the different dimensions of the aircraft and retaining tensors of a black hole to understand possible interactions between frequencies without a predefined mass and geometry that generates a high-dimensional combinatorics within a structure of superluminal aircraft and the curvature of space when using Riemann tensors.

### 2.1 The Riemann tensor

- The Riemann tensor  $R^{\sigma}_{\rho\mu\nu}$  describes the curvature of space-time. It can be calculated from the metric tensor  $g_{\mu\nu} g^{\mu\nu}$ .

### 2.2 Ricci Tensor and Scalar of Curvature

Equality Property: Two tensors  $S, T \in V^2$  are equal if and only if

$$S \cdot v = T \cdot v \quad \forall v \in V.$$

1. The Ricci tensor  $R^{\mu\nu} R^{\rho\sigma}_{\mu\nu\rho\sigma}$  is obtained by contracting the Riemann tensor:  $[R^{\mu\nu\rho\sigma} = R^{\mu\rho} R^{\nu\sigma}]$
2. The curvature scalar  $R$  is obtained by contracting the Ricci tensor:

The components of a tensor can be written in the form of a matrix,

$$[S] =$$

[S11 S12 S13

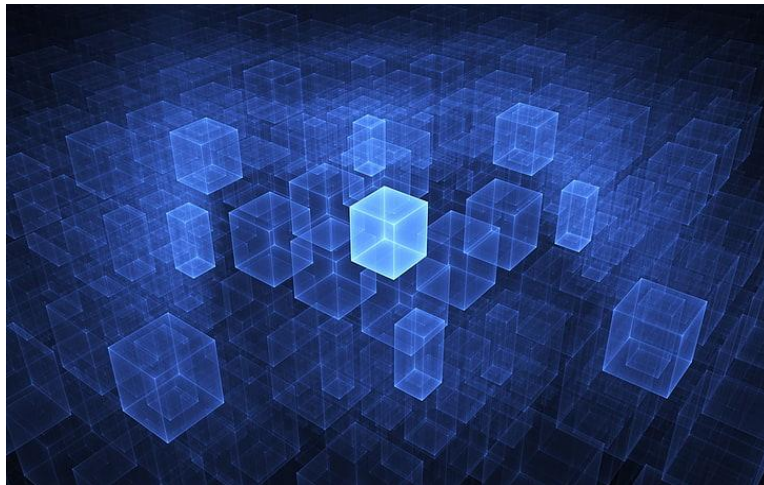
S21 S22 S23

S31 S32 S33]

, (A.15)

This basic analysis in MATLAB provides a way to study the curvature of tensors and the radiation of objects around a black hole. The steps include defining the metric tensor, computing the Christoffel and Riemann tensors, and finally, analyzing the radiation frequencies.

### Cubic representation figure of multiple spatial nodes 1.1



```
% Initial parameters
syms m q B E
v = sym('v', [1 4]); % Particle speed

% Radiation frequency calculation
gamma = 1 / sqrt(1 - norm(v)^2 / c^2); % Lorentz Factor
omega = q * B / m; % Cyclotron frequency
omega_synchrotron = gamma^2 * omega; % Synchrotron frequency
frequency
% Frequency display
fplot(omega_synchrotron, [0, 10], 'LineWidth', 2);
xlabel('Time (s)');
ylabel('Frequency (Hz)');
title('Synchrotron Radiation Frequency');
grid on;
```

The tensor product (also called dyadic) of two vectors  $\mathbf{a}$  and  $\mathbf{b}$  is defined as a tensor of order two:

$$(\mathbf{a} \otimes \mathbf{b}) \cdot \mathbf{v} = \mathbf{a}(\mathbf{b} \cdot \mathbf{v}) \quad \forall \mathbf{v} \in \mathbf{V}.$$



#### 4. Radiation Frequencies

Radiation from particles in orbit is also considered. The observed frequencies can be calculated using the synchrotron radiation formula and general relativity.

```
% Initial parameters
syms m q B E
v = sym('v', [1 4]); % Particle speed

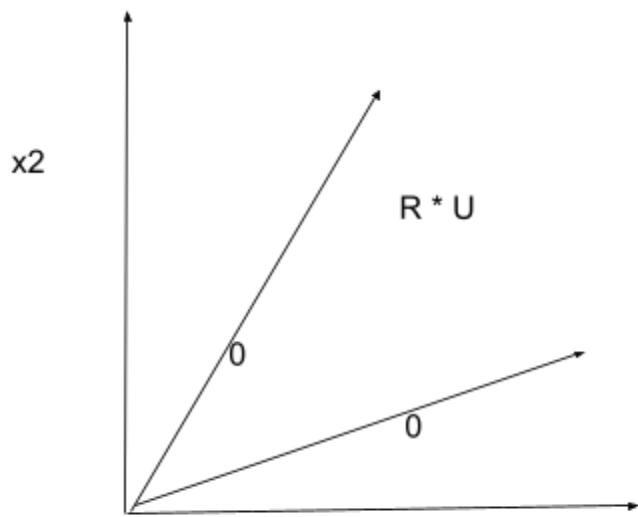
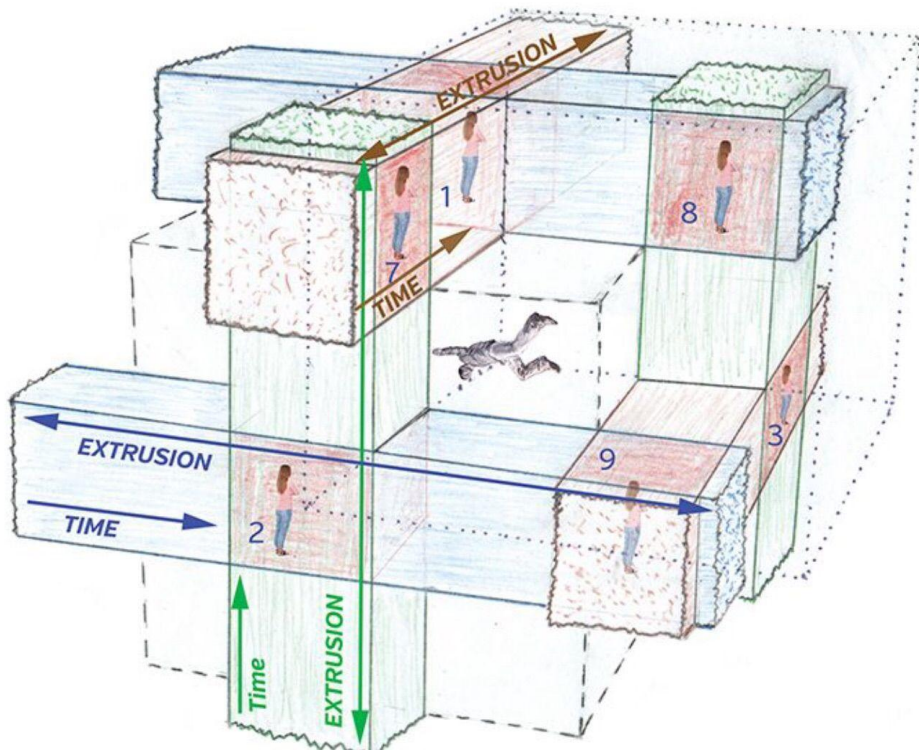
% Radiation frequency calculation
gamma = 1 / sqrt(1 - norm(v)^2 / c^2); % Lorentz Factor
omega = q * B / m; % Cyclotron frequency
omega_synchrotron = gamma^2 * omega; % Synchrotron frequency

% Frequency display
fplot(omega_synchrotron, [0, 10], 'LineWidth', 2);
xlabel('Time (s)');
ylabel('Frequency (Hz)');
title('Synchrotron Radiation Frequency');
grid on;
```

Combustible-fuel: The Variation of combustion temperature, average molecular mass of combustion gases, and theoretical specific impulse (at frozen equilibrium) as a function of oxidizer concentration for HTPB-based composite propellants. Data are for a chamber pressure of 68 atm and nozzle exit pressure of 1.0 atm. Reproduced from Ref. 13–4 with permission of the AIAA

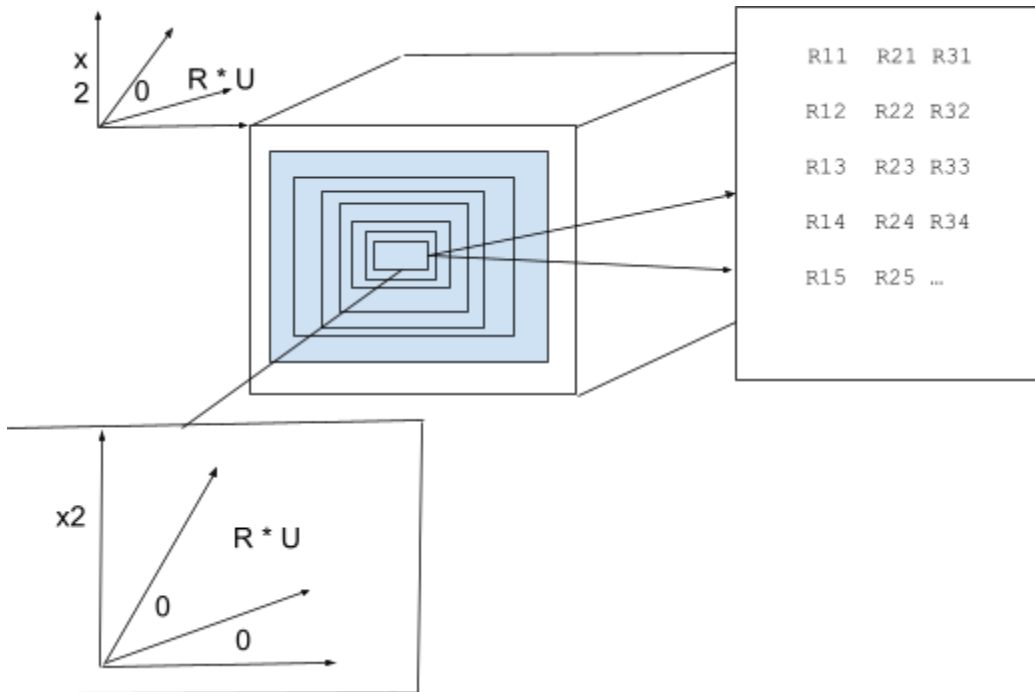
**Some of the properties of the tensors where generic structures of quantum superluminal particles are found**

1. The cube or geometric spatial shape replicates itself
2. The space and dimensions where superluminal (quantum) particles are found are deformed
3. Superluminal quantum particles transpose
4. Superluminal Quantum Particles Bend and Transform
5. Superluminal quantum particles become detached from their geometric angles
6. They do not have a defined mass or the same structure as a photon.
7. Spatial curvatures are found that are not represented in three dimensions
8. Spaces formed by particles whose behavior is not sequential, with the ability to self-modify at the tensor level
9. Spaces greater than 4 dimensions that are not visible to the eye, extremely small within tensor mathematical sets.



R11	R21	R31
R12	R22	R32
R13	R23	R33
R14	R24	R34
R15	R25	R0
R16	R26	R36
R17	R27	R37

Where R are Dimensions set  
and transitional states



The superluminal particle is represented in several dimensions and lacks the same structure and properties of a photon, structurally it is similar or bears resemblance to a qubit at a computational level, it is a series of hyper dimensions at a structural level where the particle adheres and It adapts to the set of high dimensions and frequencies of a black hole in magnetic fields or flows of five or more dimensions. These are not actually superluminal speeds, they are extra dimensions that are imperceptible and, although extremely small, they are adaptable to high-dimensional combinatorics and frequencies that cannot be accessed through the instrumentation available on this planet.

**Tensioner dimensions:**

$$R_{11} = c_1 * (R * e_1) = e_1 * (\cos\theta + \sin\theta) = \cos\theta$$

$$[R] = (\cos\theta) (-\sin\theta)$$

$$(\sin\theta) (\cos\theta)$$

## M-GLASS FIBERS AND THEIR PROPERTIES

M-glass fibers, also known as high-modulus glass fibers, exhibit significantly higher modulus values compared to standard glass fibers. Their specific modulus is notably greater than that of steel due to their lower density, which is approximately two-thirds less than steel. This enhanced modulus makes them highly suitable for structural composites, improving overall material performance.

To increase Young's modulus in  $\text{SiO}_2$ – $\text{Al}_2\text{O}_3$ – $\text{MgO}$ -based glass fibers, certain oxides such as  $\text{BeO}$ ,  $\text{Y}_2\text{O}_3$ ,  $\text{ZrO}_2$ ,  $\text{TiO}_2$ , and  $\text{CeO}_2$  are incorporated. However, due to toxicity concerns,  $\text{BeO}$  has not been widely used industrially, and  $\text{Y}_2\text{O}_3$  remains prohibitively expensive despite its effectiveness in enhancing modulus.

Chinese-manufactured "M2" glass fibers demonstrate a Young's modulus of around 95 GPa, incorporating  $\text{CeO}_2$ ,  $\text{TiO}_2$ , and  $\text{ZrO}_2$  in their composition. These fibers are known for their superior mechanical properties, including high tensile strength and durability.

## APPLICATIONS OF M-GLASS FIBERS

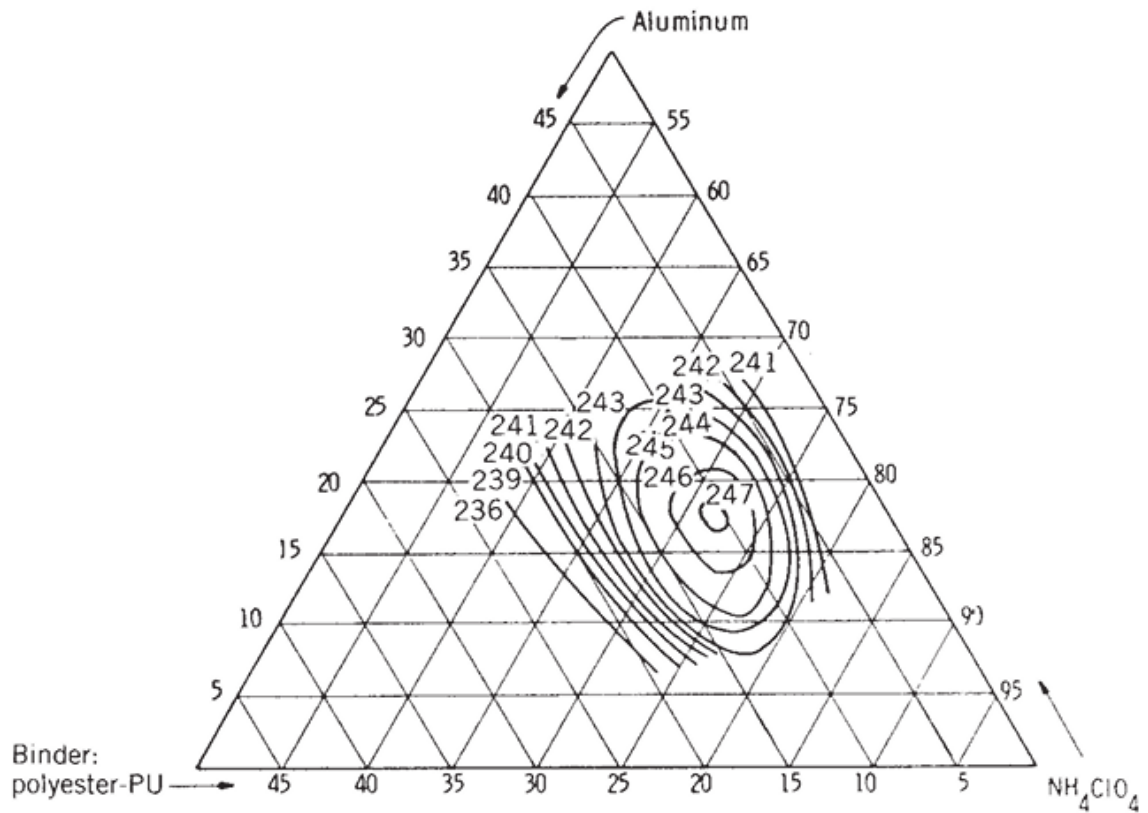
M-glass fibers are extensively utilized in advanced composite materials due to their combination of high modulus and tensile strength. These properties make them ideal for reinforcing epoxy, phenolic resins, and nylon in high-performance applications.

In aerospace industries, M-glass fibers serve as critical structural reinforcement materials, offering enhanced thermal and mechanical resistance. Additionally, their excellent insulation properties make them valuable for applications requiring superior electrical resistance.

Beyond aerospace applications, M-glass fibers have been integrated into various civil engineering projects, such as extra-high-voltage (EHV) electrical operation systems, where their insulation qualities and mechanical reliability contribute to improved operational efficiency.

The model of composites shows how the specific impulse varies with changes in the composition of the three principal ingredients: the solid AP, solid Al, and viscoelastic polymer binder. For DB propellants variations of  $I_s$  and  $T_1$  are shown in Fig. 13–5 as a function of nitroglycerine (NG) concentration. The theoretical maximum specific impulse occurs at about 80% NG. In practice, NG, which is a liquid, is seldom found in concentrations over 60% because its physical properties are poor at the higher concentrations. Other major solid or soluble ingredients are also needed to make a usable DB propellant. For CMDB propellants the addition of either AP or a reactive nitramine such as RDX allows for higher  $I_s$  than with ordinary DB (where AP or RDX percent is zero), as shown in Fig. 13–6. Both AP and RDX greatly increase the flame temperature.

The specific impulse varies with changes in the composition of the three principal ingredients: the solid AP, solid Al, and viscoelastic polymer binder. For DB propellants variations of  $I_s$  and  $T_1$  are shown in Fig. 13–5 as a function of nitroglycerine (NG) concentration. The theoretical maximum specific impulse occurs at about 80% NG. In practice, NG, which is a liquid, is seldom found in concentrations over 60% because its physical properties are poor at the higher concentrations. Other major solid or soluble ingredients are also needed to make a usable DB propellant. For CMDB propellants the addition of either AP or a reactive nitramine such as RDX allows for higher  $I_s$  than with ordinary DB (where AP or RDX percent is zero), as shown in Fig. 13–6. Both AP and RDX greatly increase the flame temperature:



Composition diagram of calculated specific impulse for an ammonium perchlorate–aluminum–polyurethane propellant (PU is a polyester binder) at standard conditions (1000 psi and expansion to 14.7 psi). The maximum value of specific impulse occurs at about 11% PU, 72% AP, and 17% Al.

## MECHANICAL PROPERTIES OF HIGH-MODULUS GLASS FIBERS

M-glass fibers, commonly used in aerospace and high-performance applications, exhibit significant variations in density, Young's modulus, and tensile strength depending on their composition and manufacturing processes.

# CHINESE HIGH-MODULUS GLASS FIBERS:

- **M1**: Density ~2.80 g/cm<sup>3</sup>, Young's modulus 93–95 GPa, specific modulus 3.32–3.39 × 10<sup>7</sup> cm, tensile strength 3.10–3.40 GPa.

- **M2**: Density ~2.77 g/cm<sup>3</sup>, Young's modulus 94–95 GPa, specific modulus 3.39–3.43 × 10<sup>7</sup> cm, tensile strength 3.20–3.81 GPa.

- **\*\*Non-Alkali Type\*\*:** Density  $\sim 2.54$  g/cm<sup>3</sup>, Young's modulus  $\sim 73$  GPa, specific modulus  $2.83 \times 10^7$  cm, tensile strength  $3.10$  GPa.

#### US-PRODUCED HIGH-MODULUS GLASS FIBERS:

- **\*\*YM31A\*\*:** Density  $\sim 2.89$  g/cm<sup>3</sup>, Young's modulus  $110\text{--}120$  GPa, specific modulus  $3.81\text{--}4.15 \times 10^7$  cm, tensile strength  $\sim 3.70$  GPa.

#### RUSSIAN HIGH-MODULUS GLASS FIBERS:

- **\*\*BM-1\*\*:** Young's modulus  $\sim 93$  GPa, specific modulus  $\sim 3.80 \times 10^7$  cm.

- **\*\*BM-100\*\*:** Young's modulus  $\sim 105$  GPa, specific modulus  $\sim 3.50 \times 10^7$  cm.

- **\*\*M-11\*\*:** Young's modulus  $\sim 112$  GPa, specific modulus  $\sim 4.30 \times 10^7$  cm.

- **\*\*M-12\*\*:** Young's modulus  $\sim 120$  GPa, specific modulus  $\sim 4.50 \times 10^7$  cm.

These materials provide high tensile strength, good thermal stability, and excellent structural reinforcement, making them valuable for aerospace, civil engineering, and electrical insulation applications. High Silica Glass Fibers High silica glass fibers contain about 96–99 wt% SiO<sub>2</sub> as well as small amounts of B<sub>2</sub>O<sub>3</sub>, Na<sub>2</sub>O and Al<sub>2</sub>O<sub>3</sub>. For the preparation of SiO<sub>2</sub>–B<sub>2</sub>O<sub>3</sub>–Na<sub>2</sub>O system glass fibers, raw materials were molten and drawn into fiber products, phase separated at 500–600 °C and then soaked in hydrochloric acid at a certain temperature. B<sub>2</sub>O<sub>3</sub> and Na<sub>2</sub>O were leached, and a porous SiO<sub>2</sub> skeleton was left; the skeleton was then sintered at 700–900 °C with the SiO<sub>2</sub> content increasing to more than 96 wt%. The high silica glass fibers have fiber diameters of 4–10 lm, a density of 2.20 g/cm<sup>3</sup>, a tensile strength of 1.50 GPa and a Young's modulus of 73 GPa. The main characteristics of these products are high-temperature stability, shape stability, thermal shock resistance and chemical stability, which enable their use as a high-temperature ablation reinforcement. For example, high silica glass fiber-reinforced phenolic resins, in various composite forms, have been used as ablation-resistant parts of missiles and rockets such as missile headgear, end skirts, shell and rocket large nozzles. High silica glass fiber carpets, fabrics and other products are superior insulation materials and can function as a thermal protection layer for missiles and rockets or as impurity filters in steel materials. In addition, because of their porous structure they can be used as catalyst supports and can be fabricated into reverse osmosis membranes for use in desalination and gas separation.

Radiation-Resistant Insulating Fibers These fibers are composed of SiO<sub>2</sub>, Al<sub>2</sub>O<sub>3</sub>, CaO and MgO and characterized by a small thermal neutron capture area, high insulation resistance, excellent mechanical properties and better water resistance than E-glass fibers. Their insulation resistance is highly stable under high doses of c-rays or strong neutron irradiation. The fibers can thus be used at high temperatures and under strong irradiation environments. For example, they can be used as main insulation materials in high-temperature cables or radiation-resistant cables in nuclear reactors. They are also insulation materials

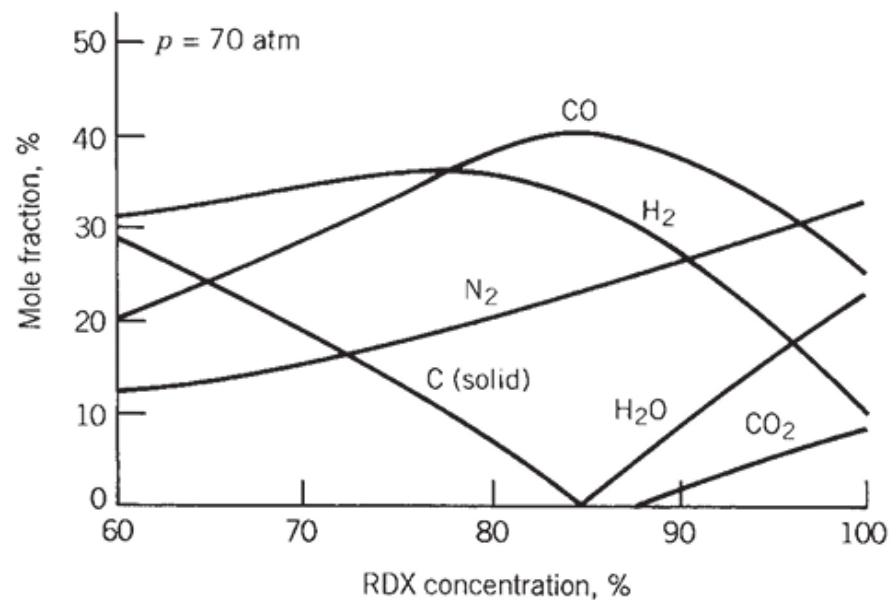
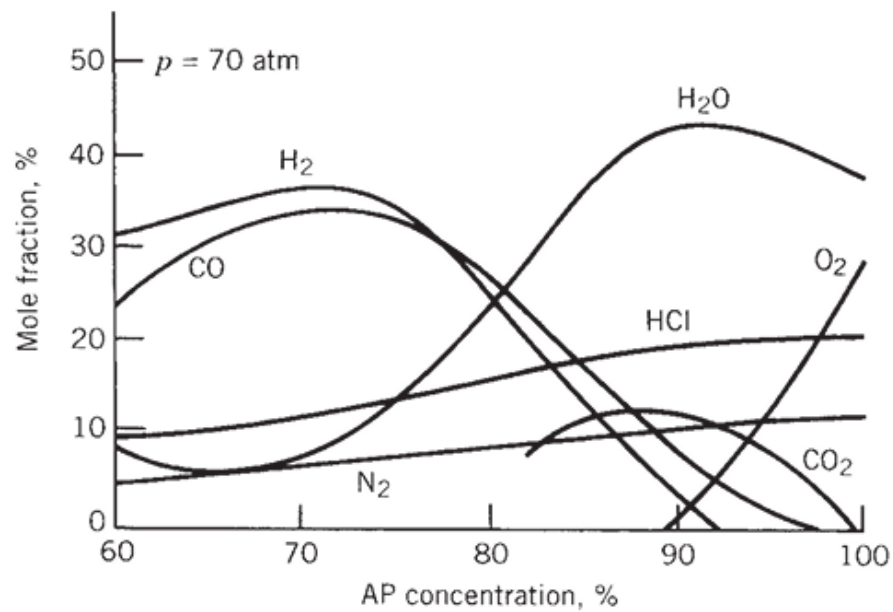
that can be used for high-temperature wires and are important reinforcements for polymer matrix composites. They can also be applied as low dielectric loss and low-density materials for electronic components or radomes.

Spacecraft attitude: tribution is axially symmetric so that  $I_{xx} = I_{yy}$ . A typical ‘spinner’ is shown in Figure 9.4. The response to a torque will be of interest in one or both of the two sets of axes. The Response in axes fixed in the structure will be of interest when the torque components are in these axes or when the attitude sensors measure components in these axes. The equations, developed from equation (3.40) of Chapter 3, are  $I_{xx} \cdot \omega_x + S\omega_y(I_{zz} - I_{xx}) = T_x$   $I_{xx} \cdot \omega_y - S\omega_x(I_{zz} - I_{xx}) = T_y$   $I_{zz} \cdot S = T_z$  Separating  $\omega_x$  from  $\omega_y$  leads to  $I_{xx}(\omega_x + \omega^2 n \omega_x) = T_x - \omega n u T_y$  and  $I_{xx}(\omega_y + \omega^2 n \omega_y) = T_y + \omega n u T_x$

PAN-CF							
Amoco T-50	6.5	1.81	2.90	300	0.7	1.61-4.09	C
T-40	5.1	1.81	5.65	290	1.8	1.88-2.7	C
T-650/35	6.8	1.77	4.55	241	1.8	0.8	C
T-300	7.0	1.76	3.45	231	1.4	2.8-2.88	C
			1.38-2.2				M
BASF							
CelionGy-70	8.4	1.90	1.86	517	0.30	1.05	C
			0.413				M
CelionG30-500	7.0	1.78	3.79	234	1.62	6.2-8.3	C
Grafil Inc.							
Grafil34-700	6.9	1.80	4.50	234	1.9	2.76	C
Grafil43-750	5.0-5.5		305		1.66-2.2		C
GrafilHM-ST	6.9-3.2		390		0.8		M
				>2.0			C
GrafilXA	7.0-3.5		230		1.39-2.0		C
PAN-CF							
Hercules							
MagnamiteHMS4	7.0	1.80	2.34	345	0.8	1.66	C
MagnamiteIM6	5.4	1.74	5.10	303	1.7	2.8-7.1	C
MagnamiteIM7	5.0	1.80	5.30	303	1.8	6.39-8.8	C
MagnamiteIM8	5.0	1.80	5.30	303	1.6	3.22	C
MagnamiteAS1	8.0	1.80	3.10	228	1.3	5.9	C
MagnamiteAS4	8.0	1.79	4.00	221	1.6	1.44	M
TohoRayon							
Besfight-HTA	7.0	1.77	3.72	235	1.6	2.8	C
				1.9			M
Toray							
Torayca-M30	6.5	1.81	1.74	392	0.6	1.6	C
Torayca-M40					1.2		M
Torayca-M40J	6.0	1.77	4.41	377	1.2	2.33	C
					3.41		C

<b>Torayca-M46</b>	6.5	1.88	2.55	451	0.6	1.4	C
						1.2	M
<b>Torayca-M50J</b>	5.0	1.80	3.92	465	0.8	4.0	C
						1.2	M
<b>Torayca-M60J</b>	4.7	1.94	3.92	588	0.7	1.67	C
<b>Torayca-T300</b>	7.0	1.75	3.53	230	1.5	2.8-3.7	C
						2.55	M
<b>Torayca-T300S</b>	7.0	1.82	4.80	230	2.1	6.1	C
<b>Torayca-T800H</b>	5.0	1.81	5.49	294	1.9	2.74-7.86	C
<b>Torayca-T1000</b>	5.0-4.8		294		2.4	2.2	M
<b>Pitch-CF</b>							
<b>Amoco</b>							
<b>ThornelP-120</b>	10.0	2.18	2.37	827	0.3	0.45	C
						0.30-0.40	M
<b>ThornelP-100</b>	10.0	2.15	2.37	758	0.3	0.48	C
						0.20-0.50	M
<b>ThornelP-75S</b>	10.0	2.00	1.90	520	0.4	0.69	C
						0.5	M
<b>ThornelP-55S</b>	10.0	2.00	1.90	380	0.5	0.85	C
						0.5	M
<b>ThornelP-25</b>	11.0	1.90	1.40	160	0.9	1.15	C
						0.5-1.4	M
<b>DuPont de Nemours</b>							
<b>FiberG-E120</b>	9.2	2.14	3.30	827	0.48	0.7	M
<b>FiberG-E105</b>	9.3	2.14	3.10	717	0.5	0.74	C
						0.80	M
<b>FiberG-E75</b>	9.3	2.14	3.10	524	0.57	0.81	C
						1.1	M
<b>FiberG-E55</b>	9.35	2.10	3.20	393	0.75	1.1	M
<b>FiberG-E35</b>	9.4	2.04	2.90	262	1.0	1.26	C
						1.60	M
<b>Mitsubishi Nippon Steel</b>							
<b>Dialead-K135</b>	10.0	2.08		201		1.2	C
<b>NT-20</b>							
<b>NT-40</b>	9.5-3.5		400		1.1-2.0		C
						1.9	M
<b>NT-60</b>	9.4-3.0		595		0.8-1.8		C
						0.7	M

**Nota:** M -measure; C - calculus



The mechanical presents a comprehensive collection of carbon fiber types used in composite materials, focusing primarily on PAN-based and pitch-based carbon fibers. These fibers differ in properties such as tensile strength, density, Young's modulus, strain capability, and compressive strength.

Starting with PAN-based carbon fibers, a wide range of commercial grades is described. For example, the Amoco T-50 fiber has a diameter of 6.5 micrometers, a density of 1.81 g/cm<sup>3</sup>, and a tensile strength of 2.90 GPa. Its Young's modulus is 300 GPa, and its strain capability varies between 1.61% and 4.09%, depending on the testing conditions. Similar materials like the T-40 and T-650/35 provide slightly lower or higher values for these properties, showing a trend in fiber optimization based on required strength-to-weight ratios.

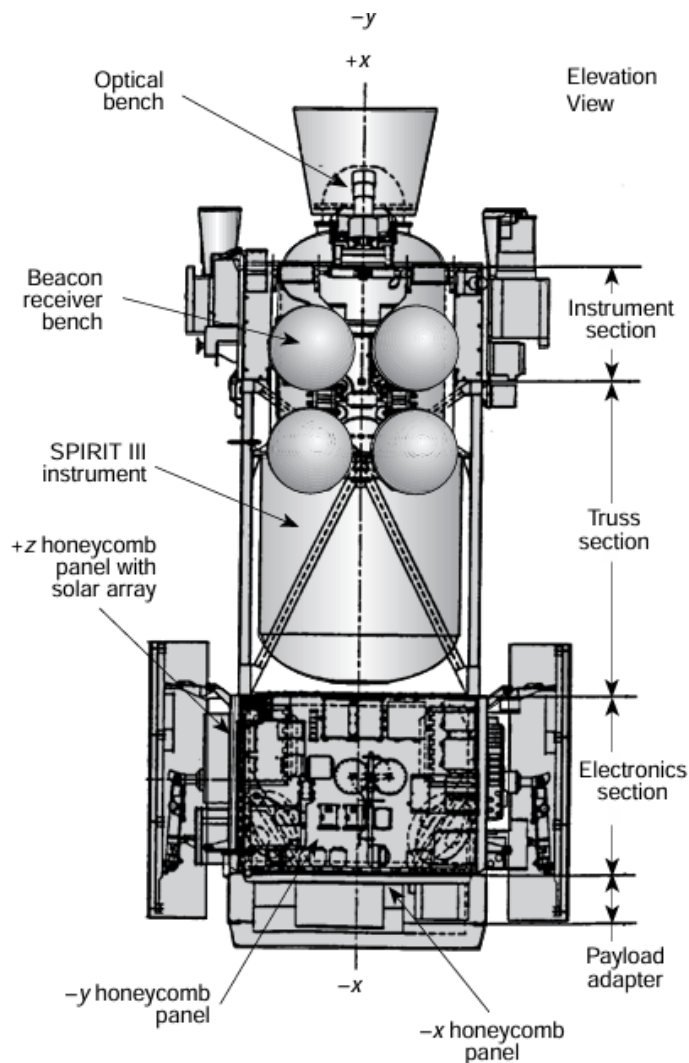
Fibers like the Celion GY-70, made by BASF, stand out due to their very high tensile strength of 8.4 GPa with relatively moderate modulus. The strain is only 0.3%, indicating high stiffness. Celion G30-500 has a broader strain range and higher compressive strength.

Grafil Inc. offers several grades, including the Grafil 34-700 and Grafil 43-750. These show tensile strengths in the range of 4.5 to 5.5 GPa, with modulus values between 230 and 305 GPa. The strain and compressive strength vary by grade, reflecting specific application suitability—whether for structural rigidity or energy absorption.

Hercules Magnemite series includes the IM6, IM7, and IM8 grades. These are well-known high-modulus carbon fibers with strengths exceeding 5 GPa and moduli around 303 GPa. Strains range between 1.6% and 1.8%, with compressive strengths of up to 8.8 GPa in some cases.

Toray, one of the leading Japanese producers, contributes various models such as Torayca M30, M40J, and T300. For instance, the M40J offers a high modulus of 377 GPa, a tensile strength of 4.41 GPa, and a moderate strain of 1.2%. Their M60J reaches a Young's modulus of 588 GPa, suitable for high-stiffness needs like aerospace applications.

Pitch-based fibers, such as Amoco's Thorne series (P-25, P-55S, P-75S, P-100, and P-120), are highlighted for their very high modulus, especially in grades like P-120 with over 800 GPa. However, these fibers usually exhibit lower strain tolerance, often below 0.5%, making them extremely stiff but brittle in comparison to PAN-based fibers.



DuPont offers the Fiber G-E series, which combines pitch-based precursors with specific enhancements. For example, G-E120 has a modulus of 827 GPa and strain around 0.48%. This series typically shows higher density and compressive strength, favorable in electronics and structural damping.

Mitsubishi and Nippon Steel offer the NT series (NT-20, NT-40, NT-60), which also fall under pitch-based categories. They are characterized by varying diameters and compressive strengths, usually in the range of 400–600 MPa, suitable for applications requiring thermal stability and electrical conductivity.

In addition to mechanical data, the document discusses horizontal compressive strength, shear modulus, damping factors, and horizontal compressive modulus. For instance, Torayca T300 shows a horizontal compressive strength of 556 MPa, a strain of 26%, a shear modulus of 15 GPa, and a damping factor of 1.30.

Applications of carbon fiber composites are wide-ranging: aerospace and transportation benefit from their high strength and low weight. Missiles and aircraft braking systems rely on the low thermal expansion and high dimensional stability. Audio and robotic applications use them for their excellent damping and stiffness. In medical and electrical domains, their X-ray transparency and conductivity play vital roles. Chemical processing environments leverage their resistance to corrosion.

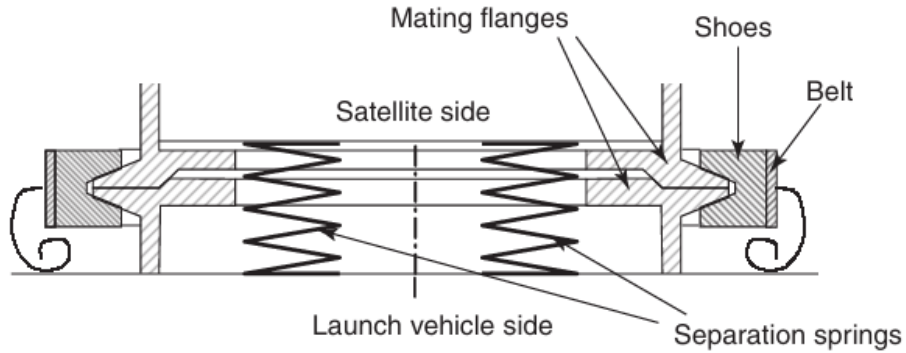
In terms of origin, PAN-based carbon fibers dominate the global market, contributing approximately 80% of total carbon fiber output. Around 70% of these fibers are produced by Japanese companies like Toray, Toho, and Mitsubishi. The rest comes from producers in the U.S., such as Hexcel and BP Amoco, as well as China's Formosa Plastics.

Lastly, the document introduces mechanical properties for carbon yarns produced in China and Japan. These include MT and HT-I from China with moderate tensile strengths (2.06 and 2.56 GPa) and lower modulus values. Japan's T300 and M40 offer improved strength and stiffness, further illustrating regional expertise.

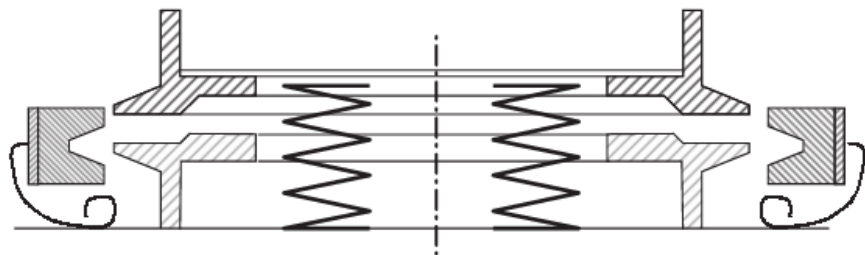
Different precursors used in carbon fiber production yield varying mechanical profiles. PAN-derived fibers tend to offer a balanced profile with tensile strengths ranging from 3.5 to 8.0 GPa and moduli from 230 to 600 GPa. Rayon-based fibers offer low strength and modulus but relatively higher strain, while pitch-derived fibers provide high stiffness with lower elongation. Overall, the document provides a detailed catalog of industrial carbon fiber products.

Pure-spin spacecraft The dynamics of a spinner are covered in Section 3.4.2 of Chapter 3. It is assumed here that the whole vehicle is spinning about its z-axis with an angular rate  $S$ , and that its mass distribution is axially symmetric so that  $I_{xx} = I_{yy}$ . A typical ‘spinner’ is shown in Figure 9.4. The response to a torque will be of interest in one or both of the two sets of axes. The Response in axes fixed in the structure will be of interest when the torque components are in these axes or when the attitude sensors measure components in these axes.

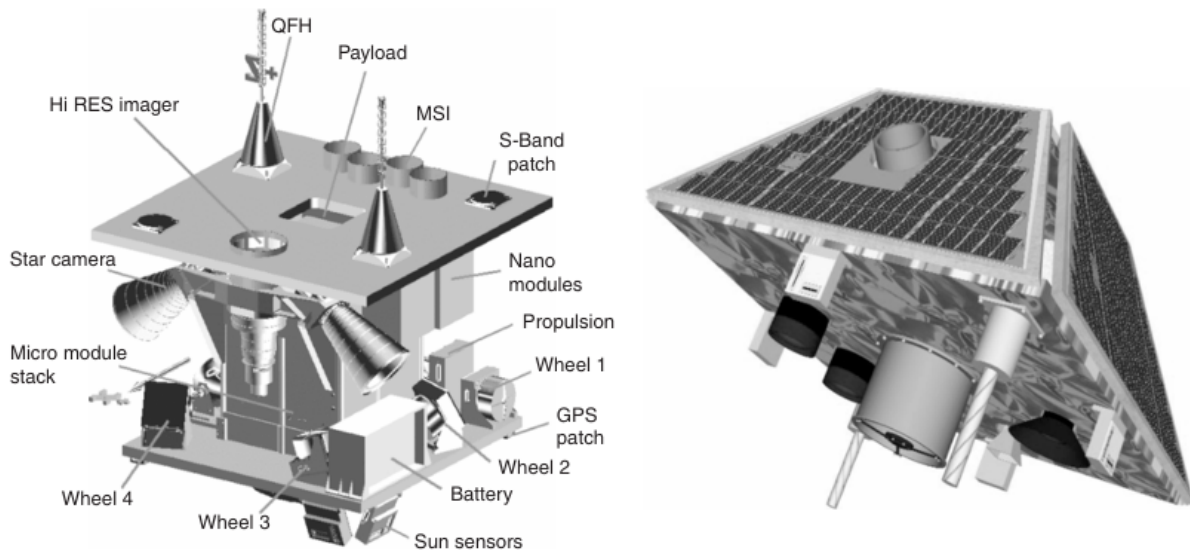
The equations, developed from equation (3.40) of Chapter 3, are  $I_{xx} \cdot \omega_x + S\omega_y(I_{zz} - I_{xx}) = T_x$   $I_{xx} \cdot \omega_y - S\omega_x(I_{zz} - I_{xx}) = T_y$   $I_{zz} \cdot S = T_z$  Separating  $\omega_x$  from  $\omega_y$  leads to  $I_{xx}(\omega_x + \omega_n \nu \omega_x) = -T_x - \omega_n \nu T_y$  and  $I_{xx}(\omega_y + \omega_n \nu \omega_y) = -T_y + \omega_n \nu T_x$  (9.3) (9.4) where  $\omega_n \nu = S[(I_{zz}/I_{xx}) - 1]$  is the frequency (rads/s) of the nutation mode referred to in Section 3.4.2 of Chapter 3, when observed in the spacecraft’s axes. This mode will need to be damped, whereupon the eventual constant components  $\omega_x$ ,  $\omega_y$  in response to constant torques  $T_x$ ,  $T_y$  will become  $\omega_x = -T_y/S(I_{zz} - I_{xx})$  and  $\omega_y = T_x/S(I_{zz} - I_{xx})$  (9.5) When these are combined with the spin motion, the result is a coning rotation of the z-axis at the spin frequency  $S$  when viewed from outside the spacecraft. One of the major reasons for spinning a spacecraft is to counter the effect upon the trajectory that is caused by a thrust offset when a high-thrust motor is being used, such as during orbit-changing manoeuvres.



(a) Mechanism closed

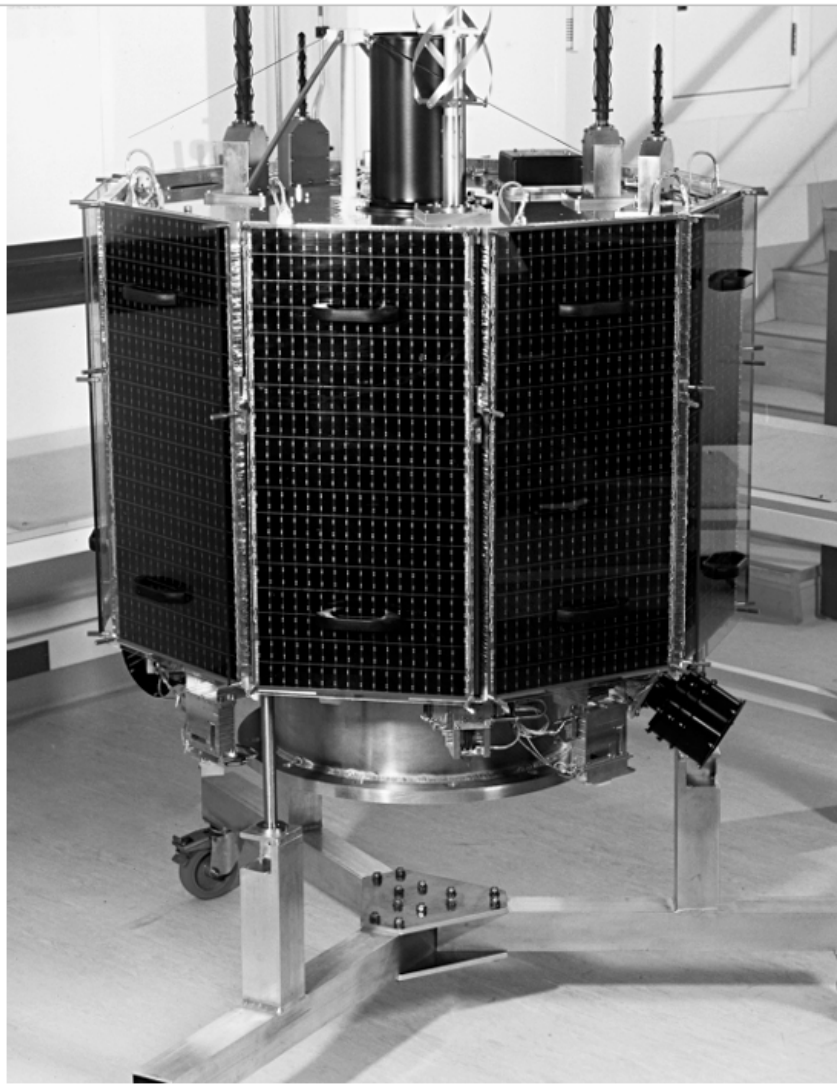


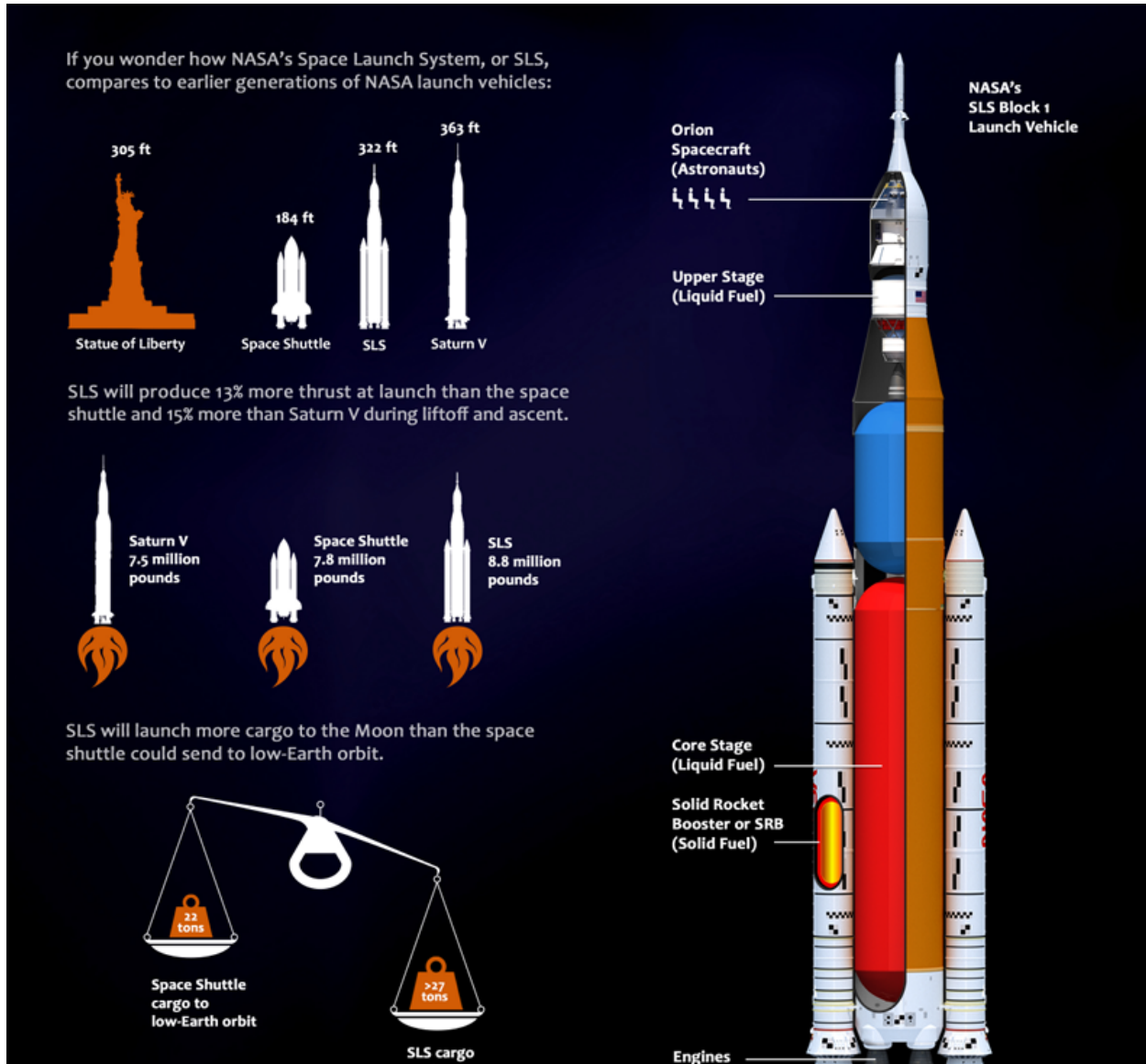
(b) Mechanism opened



There has been a steady stream of primarily scientific and military satellites in the few 100kg ‘minisatellite’ class. Since the early 1990s a number of such satellites have been built for just a few tens

of millions of dollars—low by conventional space standards. However, in response to growing payload demands for power, volume and mass—but within very small-scale financial budgets—there has been increasing interest in flying minisatellites constructed on the same principles as the microsatellites previously described. SSTL's first mini-satellite platform, shown in Figure 18.10, was designed according to such cost-effective principles—resulting in a basic platform cost of £5–6 million In an age of decommissioning of nuclear weapons, it is interesting to note that UoSAT 12 was launched successfully by a converted SS-18 (Dnepr) Inter-continental Ballistic Missile (ICBM). Three-axis control was provided by a combination of magnetor quers, momentum wheels and cold gas N2 thrusters—whilst an experimental electric N2O resisto-jet thruster provided orbit trimming and maintenance demonstrations for future network constellations. Much of the technology proved on this mission has been incorporated into the current-generation of enhanced microsatellites—demonstrating the important inter-play between technology demonstration missions and the development of operational spacecraft.





## STRUCTURAL DESIGN OF THE MSX SPACECRAFT

by aluminum honeycomb panels. The interior and exterior of the honeycomb panels are densely populated with electronics packages used to power and operate the spacecraft subsystems. In addition to providing the square-to-round transition necessary to mate the spacecraft to the launch vehicle, the payload adapter provides an overflow location for mounting electronics packages and the electrical umbilical connections to the spacecraft.

The skeletal frame of the electronics section is composed of several intricately machined aluminum structural shapes and fittings that were precisely aligned and assembled using special high-tensile-strength fasteners. The assembled frame includes a unique triangularly shaped bracket used to mount the attitude control subsystem's reaction wheels in each inside corner. The reaction wheel bracket was designed to precisely align the wheel's axis of rotation at 0.44 rad to the y/z spacecraft axes. The 0.44-rad inclination of the four reaction wheels provides redundant attitude and guidance control of the spacecraft in the event of a single reaction wheel failure.

The base of the frame includes a specially machined base plate that initiates a smooth transition from the square cross section of the electronics section to the round cross section of the Delta II launch vehicle. The transition is completed by attaching a cylindrical payload adapter fitting to the underside of the frame baseplate. The skeletal frame was designed and fabricated at APL. Parts of the electronic section frame, the reaction wheel bracket, and the baseplate can be seen in Fig. 3.

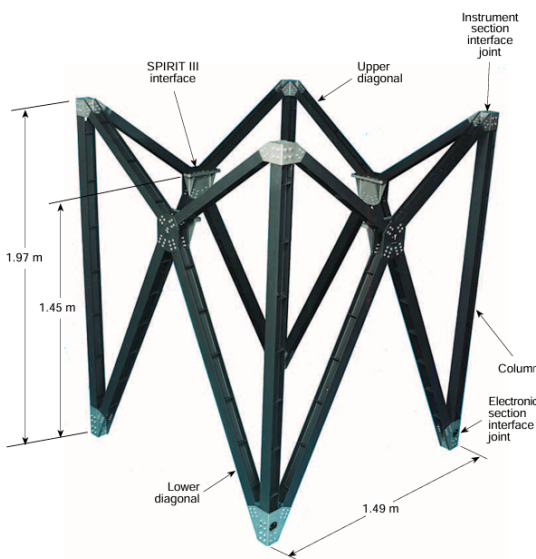
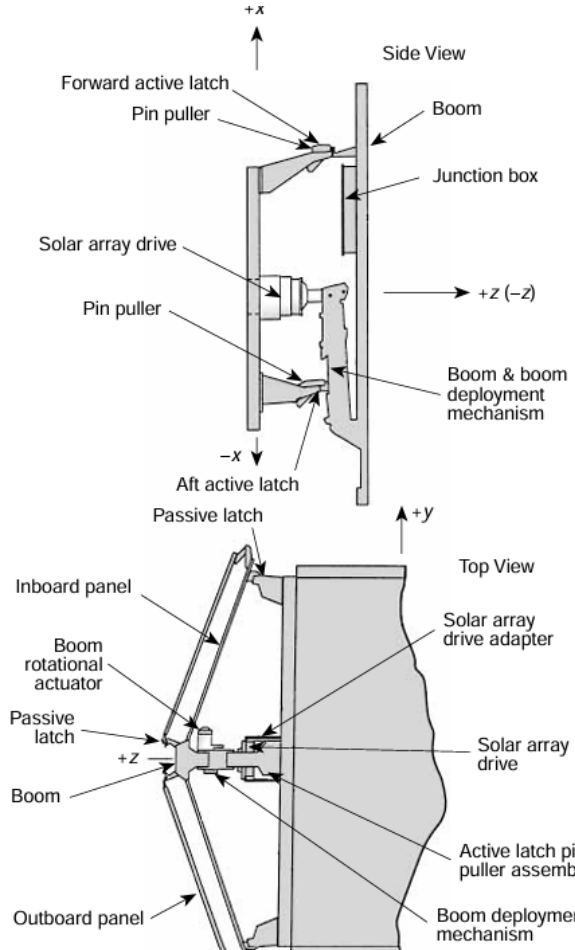


Figure 6. MSX truss structure.



The four sides ( $\pm y$  and  $\pm z$  axes as shown in Fig. 2) and the bottom ( $2x$  axis) opening in the frame are covered by 5.2-cm-thick aluminum honeycomb panels with 0.6-mm-thick aluminum face sheets and integral machined edge members. The honeycomb panels are individually bolted to the faces of the frame to provide the lateral stiffness required for the entire assembly. The electronics section was designed so that the honeycomb panels on the  $\pm z$  axes sides of the spacecraft can be removed to provide access to the interior of the frame.

The hollow center of the frame is used to house several attitude control and data storage devices. Figure 3 shows the interior of the electronics section frame as viewed with the  $+z$  honeycomb panel removed. Visible inside the frame are the following devices:

- Four each Reaction wheel assemblies mounted on triangularly shaped brackets in all four lower corners.

- Three each Torque rod assemblies mounted on the inside surface of the 2x axis and +y axis honeycomb panels.
- One each Reaction wheel control electronics package mounted on the inside surface of the 2x axis honeycomb panel.
- Two each Tape recorder assemblies (composed of separate electronics and recorder packages) mounted on the inside surfaces of the  $\pm z$  axes honeycomb panels.

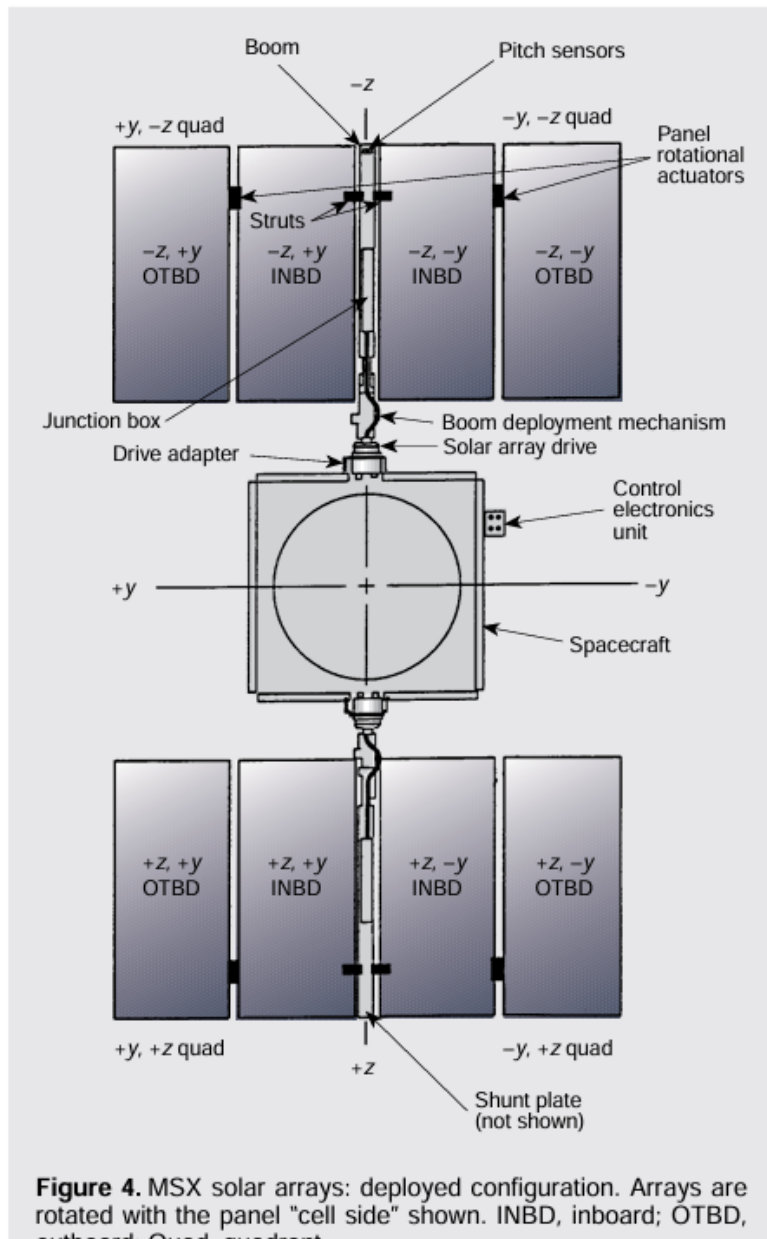
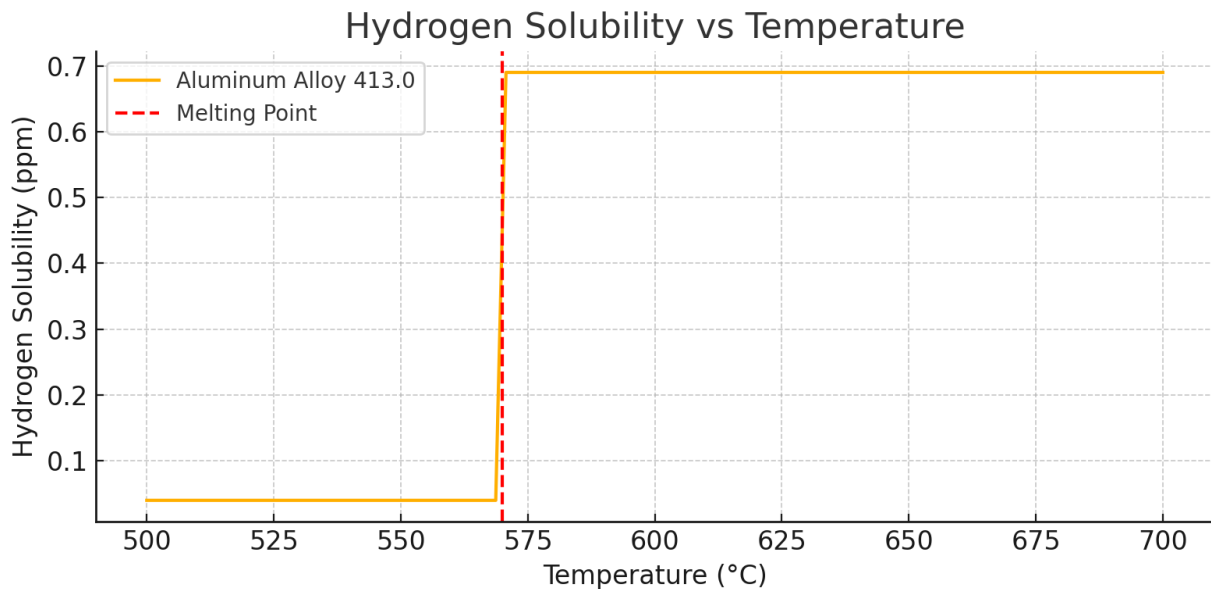


**Figure 4.** MSX solar arrays: deployed configuration. Arrays are rotated with the panel "cell side" shown. INBD, inboard; OTBD, outboard; Quad, quadrant.

The exterior surfaces of the  $\pm y$ ,  $\pm z$ , and  $2x$  axes honeycomb panels are used to mount an assortment of electronics packages, communication antennas, solar arrays, batteries, and associated support brackets. The honeycomb panels contain threaded inserts, bonded integral with the panel, used to attach the flight packages. The  $+x$  axis side of the electronics section is covered by two half panels, each 1.4 cm thick with 0.6 mm-thick aluminum face sheets and integral spools for attachment to the panels. This structure is primarily required to provide the necessary in-place stiffness for the top of the electronics section structure.



**The cylindrical payload adapter was designed jointly by APL and McDonnell Douglas Aerospace and fabricated by McDonnell Douglas Aerospace.** The adapter, which completes the transition of the frame from the square-to-round cross section, is 1.60 m in diameter by 0.30 m long with a skin thickness of 4.3 mm. The upper flange of the adapter contains a 48-hole bolt circle that attaches to the baseplate of the frame with special high tensile-strength fasteners. The lower flange

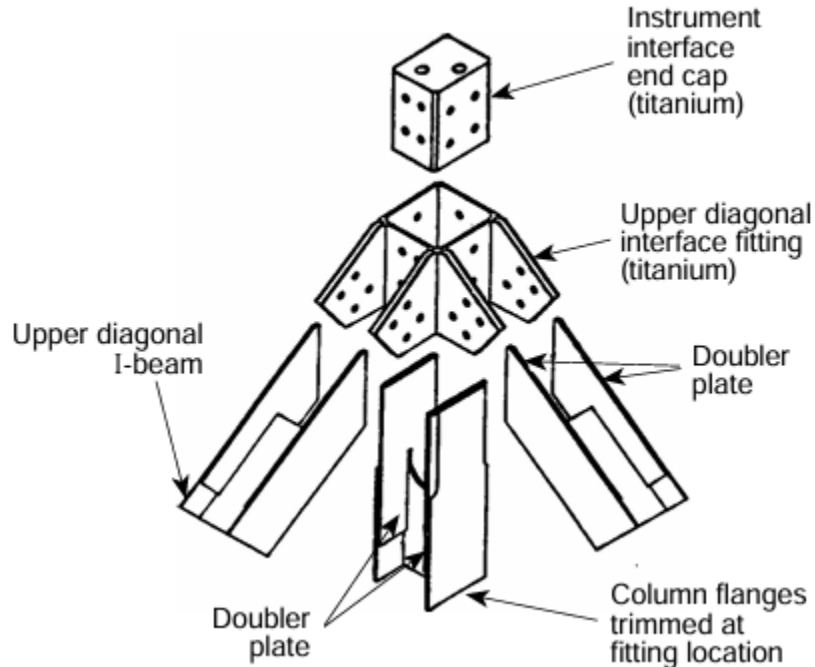
of the adapter is machined to mate with the McDonnell Douglas 6306 payload attach fitting and separation clamp band assembly. The hollow center section of the adapter surrounds the electronics packages mounted to the exterior surface of the 2x axis honeycomb panel.

The primary hardware mounted in this area includes the spacecraft battery and power distribution electronics packages.

The truss structure designs are stiffness (space craft frequency of 12 Hz lateral and 35 Hz axial), rotational stability of the SPIRIT III mounting plane ( $0.01^\circ$ ), mass (less than 54.4 kg), and strength (maintain positive margins of safety). A low coefficient of thermal expansion (CTE) (0.54 3 1026 in./in. per  $^\circ\text{C}$ ) and control of dimensional changes caused by absorption and desorption of moisture were required to achieve the stability requirement. A low thermal conductivity (less than 5.0 W/m $\cdot$  $^\circ\text{C}$ ) was necessary to minimize the heat transfer between the electronics and instrument sections. Additional requirements considered in the development of this unique part of the MSX structure included stability performance when exposed to temperature gradients as a result of the colder than normal temperature environment (+y side, 278°C; 2y side, 267°C; +z side, 271°C; 2z side, 267°C), survival as a result of temperature extremes (290°C to +90°C), and a grounding impedance of  $\leq 50$  mV. This combined set of requirements necessitated the use of Inadvertent Ignition If a rocket motor is unexpectedly ignited and starts combustion, the very hot exhaust gases may cause burns and local fires, or ignition of adjacent rocket motors. Unless the motor is constrained or fastened down, its thrust will accelerate it to unanticipated high velocities or erratic flight paths that can cause much severe damage.

Its exhaust cloud can be toxic and corrosive. Inadvertent ignitions may be caused by the following effects: Stray or induced currents that activate the igniter. Electrostatic charging causes unintended sparks or arc discharges. Fires excessively heating rocket motor exteriors, raising the solid propellant temperature above its ignition point. Impacts (bullet penetration or dropping the rocket motor onto a hard surface). Energy absorption from prolonged mechanical vibrations that overheat the propellant (e.g., transport over rough roads). Radiation from nuclear explosions. An electromechanical system called safe and arm system is usually included to prevent stray currents from activating the igniter. It averts ignition induced by currents in other wires of the vehicle, radar- or radio-frequency-induced currents, electromagnetic surges, or pulses from nuclear bomb explosion. It prevents any electric currents from reaching the igniter circuit during its “unarmed” condition. When in the “arm” position, it accepts and transmits a start signal to the igniter. Electrostatic discharges (ESD) may be caused by lightning, friction in insulating materials, or by the moving separation of two insulators. The buildup of high electrostatic potentials (thousands of volts) may, upon discharge, allow rapid increases in electric current, which in turn may lead to arcing or exothermic reactions along the current’s path. For this reason all propellants, liners, or insulators need to have sufficient electric conductivity to prevent any buildup of such an electrostatic charge. The well-known inadvertent ignition of a Pershing ground-to-ground missile is believed to have been caused by an electrostatic discharge while in the transporter-erector vehicle. ESD capabilities depend on materials, their surface and volume resistivities, dielectric constants, and the breakdown voltages.

Viscoelastic propellants are excellent absorbers of vibration energy and can become locally hot when oscillating for extensive periods at particular frequencies.



## INSTRUMENT SECTION

The truss elements were made from a T50/ERL1962 G/E composite material configured in a pseudo isotropic laminate stacking sequence of (02°/60°/260°)S3. T50 graphite fibers were chosen because of their minimal thermal conductivity and high stiffness characteristics. Amoco's ERL1962 resin was selected because it is a toughened resin system that has excellent mechanical properties and exhibits good resistance to microcracking. Composite materials can be tailored to enhance performance.

The MSX instrument section must provide a thermally stable platform to accurately support the majority of MSX instruments. This structure was designed to minimize Sun-induced thermal gradients that would vary the co-alignments of the instruments during various spacecraft observations and maneuvers. The instrument section suite includes the Ultraviolet and Visible Imagers and Spectrographic Imagers experiment (nine spectrographs and imagers), two horizon sensors, three digital solar attitude detectors, a xenon lamp, a total pressure sensor, a mass spectrometer, four temperature-controlled quartz crystal microbalances, a krypton lamp, the Space Based Visible Telescope, six reference object canisters, and several electronics packages. The instrument section assembly is shown installed in the MSX spacecraft at the top of Fig. 1.

The instrument section structural design consists of machined aluminum structural members joined together to form a large "box"-style frame similar to that of the electronics section. It interfaces with the

truss structure at four corners and provides the four lift points for the spacecraft. The structural elements of the framework consist of “L”-shaped edge members and “U”-shaped center members joined with intricately machined corner fittings and fasteners. The center members are used on the y and z sides to provide additional framework rigidity and support for the instrument honeycomb panels. The instrument section frame structure measures  $1.59 \times 1.59 \times 0.72$  m and is also used for attaching secondary structures that mount several SPIRIT III electronic chasses and the optical bench.

Very precise controls on tolerances and size were required on the internal frame assembly to minimize tolerance buildups as panels, instruments, and other parts of the structure were attached at later dates. The structure was assembled using a large granite table, custom-fabricated squares, and tooling to maximize the flatness, parallelism, and perpendicularity of all sides. After all the structural parts of the frame were assembled and adjusted, the assembly was match-drilled and permanent shear and tension Hi-Lok fasteners were installed. The assembly process produced an extremely precise finished structure for mounting the instrument honeycomb panels.

**Table 1. Material properties of T50/ERL1962:**

- Tensile strength (0°/90°):  $4.34/3.46 \times 10^8$  N/m<sup>2</sup>
- Tensile modulus (0°/90°):  $8.69/9.28 \times 10^{10}$  N/m<sup>2</sup>
- Tensile Poisson ratio (0°/90°): 0.30/0.34
- Compression strength (0°/90°):  $3.29/3.34 \times 10^8$  N/m<sup>2</sup>
- Compression modulus (0°/90°):  $8.07/8.83 \times 10^{10}$  N/m<sup>2</sup>
- Compression Poisson ratio (0°/90°): 0.32/0.33
- Flatwise tensile:  $1.17 \times 10^7$  N/m<sup>2</sup>
- Two-rail shear:  $2.25 \times 10^8$  N/m<sup>2</sup>
- Short beam shear:  $7.34 \times 10^7$  N/m<sup>2</sup>
- CTE (0°/90°):  $0.56/0.45 \times 10^{-6}$  in./in./°C

The honeycomb panels, which are attached to the frame structure on the four sides ( $\pm y$  and  $\pm z$ ) of the spacecraft, presented several design challenges primarily related to the thermal requirements. Each of these panels is a 3.3-cm-thick rectangular-shaped aluminum honeycomb panel with 0.5-mm aluminum face sheets, and each contains three embedded heat pipes for transferring heat from the instruments to the radiator assemblies. Many of the threaded spool inserts used to mount the instruments are attached directly to the heat pipes, thus providing a conductive heat path to the radiator assemblies.

In addition, the +y side panel heat pipes extend beyond both edges of the panel in order to interface with the radiator assemblies mounted on the +z and -z panels. The -y side panel contains few packages; thus heat is transferred through the frame via conduction. Smaller packages that were not well defined when the panels were fabricated are to be attached to the panels with surface-mounted rivenuts installed at a later date. The side-panel internal surfaces were masked and painted with Z306 Chemglaze paint to augment radiating capabilities, thus enhancing isothermal performance.

The panels and frame were then coated with thermal grease to maximize heat transfer between the panels and frame. Special “Milson” close-tolerance, high-strength fasteners are used to attach the panels to the frame structure. These fasteners prevent movement of the panels relative to the frame under load. They also provide accurate repositioning of the panels should they need to be removed and reinstalled.

Four “half-moon”-shaped honeycomb panels close out the top and bottom of the instrument section structure and provide additional rigidity and in-plane stiffness to the structure. All panels are made from 2-cm-thick aluminum honeycomb with 0.5-mm-thick face sheets. They are designed to be removed to facilitate the installation of the SPIRIT III instrument and provide adequate clearance around the instrument when installed. In addition, the top panels (+x side) contain embedded structural members used for attaching the six reference object canisters.

**Table 2. MSX spacecraft limit load factors (Delta II):**

- Thrust (x) axis: Liftoff 22.4 g / MECO +0.2 g
- Lateral (y, z) axes:  $\pm 2.5$  g
- Liftoff: 27.1 g
- MECO: —  
*(Note: Loads are applicable at the spacecraft's center of gravity. “—” implies compression to launch vehicle interface.)*

To meet instrument co-alignment requirements, the total structural and on-orbit distortion for all of the structure above the SPIRIT III mounting interface was not to exceed  $0.042^\circ$ . This represents a combined mechanical and thermal loads problem that directly affected the design of the truss and instrument section structures.

## Case Overpressure and Rocket Motor Failure

A rocket motor case may rupture or explode during operation when the chamber pressure exceeds the case’s burst pressure. The release of high-pressure gases can result in violent explosions, propelling fragments of the motor into surrounding areas.

A sudden depressurization from chamber pressure to ambient pressure (typically below the deflagration limit) will generally halt combustion in a Class 1.3 propellant (see *Hazard Classification*). Large pieces of unburned propellant are often found following such violent case failures.

## Common Causes of Case Overpressure

1. Propellant grain is degraded:
  - The grain may be overaged, porous, severely cracked, or have large unbonded areas due to accumulated damage.
2. Chemical changes in the propellant:
  - Caused by migration or slow, low-order chemical reactions that:
    - Reduce mechanical properties.
    - Cause grain weakening, cracking, or uncontrolled increases in the burning rate.
    - Generate gaseous by-products that form small voids, increasing internal pressure—especially dangerous in sealed, stored motors.
3. Manufacturing defects:
  - Result from poor fabrication or insufficient inspection.
4. Physical damage to the motor case:
  - For example, a nick or dent from improper handling weakens the case.
  - Can be prevented through careful handling and repeated inspections.
5. Nozzle obstruction:
  - A large loose piece (e.g., insulation) can block the nozzle, causing rapid pressure buildup in the chamber.
6. Moisture absorption in hygroscopic propellants:
  - Weakens strength and strain capabilities by factors of 3 to 10.
  - Motors are typically sealed to prevent humid air exposure.

---

## Deflagration and Detonation

When an overpressurized propellant grain ignites, it may either **continue burning (deflagration)** or **explode violently (detonation)**. Table 13-4 compares the key characteristics of each process:

Characteristic	Burning with Air	Deflagration within Rocket Motors	Detonation of Rocket Motor
Typical material	Coal dust and air	Propellant (no air)	Rocket propellant or explosives
Common initiation method	Heat	Heat	Shockwave + heat
Linear reaction rate (m/sec)	$10^{-6}$ (subsonic)	0.2 to $5 \times 10^{-2}$ (subsonic)	2 to $9 \times 10^3$ (supersonic)
Shockwaves	No	No	Yes
Reaction completion time (sec)	$10^{-1}$	$10^{-2}$ to $10^{-3}$	$10^{-6}$
Maximum pressure [MPa (psi)]	0.07-0.14 (10-20)	0.7-100 (100-14,500)	7,000-70,000 ( $10^6$ - $10^7$ )
Limiting factor	Heat transfer	Case strength	Material properties
Increase in burning rate may cause	Furnace failure	Case overpressure and explosive failure	Total case failure and complete propellant explosion
Remaining material	Unburned dust pockets	Unused propellant pieces (often stop burning)	No propellant remains
Classification	None	Class 1.3	Class 1.1

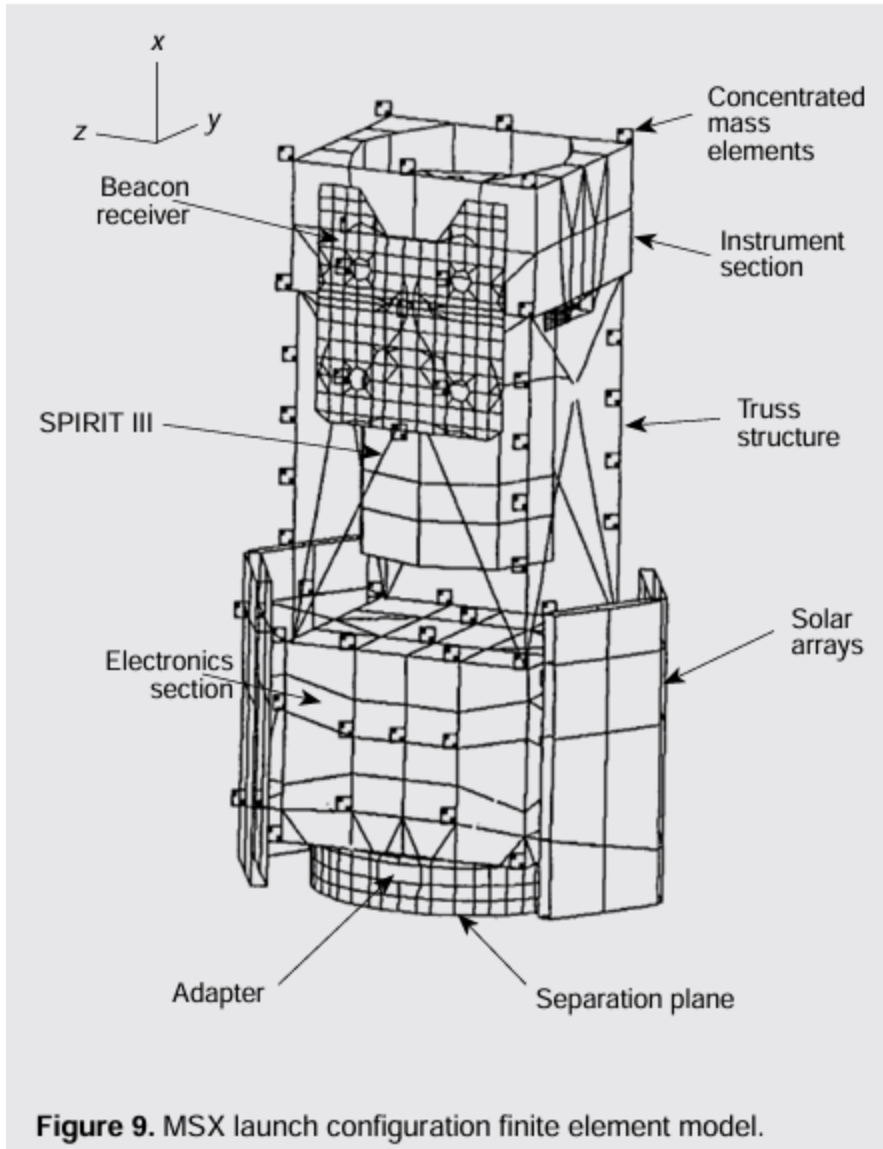


**Figure 9.** MSX launch configuration finite element model.

### Structural Testing and Verification of the MSX Spacecraft

Due to the physical constraints of the MSX spacecraft, full system-level structural testing was not feasible. Instead, static load tests were carried out on each major structural segment of the spacecraft. These structural elements were proof-tested to ensure they could withstand worst-case expected flight loads, with an additional 25% margin for safety. Testing scenarios simulated the most critical loading conditions on structural members.

Strain gauges and deflection indicators were employed throughout each test sequence to monitor stress levels in key elements, ensuring that the design stress limits were not exceeded. The collected data was used to validate and calibrate the finite element model (FEM) of the spacecraft used during the prior structural analysis phase.

Each of the spacecraft's instrument and electronics sections underwent two separate test procedures. The first test (illustrated in Fig. 10) verified the integrity of corner fittings and load attachments simulating conditions such as flight and lifting. Tensile forces of 4535 kg and 1135 kg were applied at each corner for the electronics and instrument sections, respectively.

The overall structural integrity was confirmed through combined lateral and compressive loads (see Fig. 11). Lateral forces of 9070 kg and 1815 kg, and compressive forces of 2040 kg and 726 kg, were applied in four orthogonal directions for the electronics and instrument sections respectively, to ensure all possible loading scenarios were covered. Test results showed that both sections had sufficient strength to survive maximum anticipated flight loads. While the measured stress values were lower than predicted and deflections slightly higher, these deviations were attributed to slippage between the frame and honeycomb panels.

A separate test on the truss section (Fig. 12) focused on the most critical component—the lower diagonal member. A compressive load of 4322 kg was applied. Though the intended loading was achieved, the observed lateral deflection was 2.5 times higher than expected. The discrepancy was attributed to:

- Modeling inaccuracies,
- Movement of the truss relative to the test floor, and
- Rigid body rotation of the truss/base assembly.

These findings were incorporated into the analytical model to confirm that they would not adversely affect the spacecraft's structural loading under actual conditions.

---

## Structural Margins and Dynamics

Table 3 summarizes the minimum margins of safety for each primary structural element of the MSX spacecraft. Table 4 defines the system's fundamental dynamic modes. While the spacecraft's natural frequencies (8.4 Hz for bending, 29.9 Hz for axial mode) did not meet Delta II launch vehicle guidelines (12 Hz and 35 Hz), a coupled load analysis conducted by McDonnell Douglas confirmed that the limit load factors (as presented earlier in Table 2) remained unchanged.

Once manufactured, all primary structural components were subjected to structural performance validation. FEM simulations showed that maximum thermal-induced distortions in orbit were under 0.02°.

---

## Optical Bench System

During science missions, alignment shifts between components mounted on the optical bench—two ring laser gyros, one star camera, and two autocollimators—had to remain within:

- 2 arcseconds of relative angular rotation, and
- 0.0254 mm of relative displacement,

to maintain accurate alignment with the SPIRIT III instrument boresight. Any unmeasured rotational movement would introduce systematic errors. Therefore, a highly precise and stable structural platform was necessary.

Conventional materials like aluminum were inadequate, leading to the selection of a graphite/epoxy (G/E) composite. To maintain thermal stability:

- The operational on-orbit temperature is regulated at 20°C,
- Thermal gradients are controlled to within 1°C, both in-plane and through the bench thickness,
- The Coefficient of Thermal Expansion (CTE) goal for the laminate was 0.0, and
- Rigid-body rotation was limited to  $\leq 0.006^\circ$  (22 arcsec).

These constraints led to the development of a unique kinematic mounting system, ensuring minimal rotational transmission from the spacecraft structure to the optical bench.

The optical bench is mounted atop the instrument section near the SPIRIT III aperture. The structure:

- Weighs 4.45 kg,
- Measures 0.34 m  $\times$  0.97 m  $\times$  0.038 m, and
- Is a sandwich construction with a rib core and face sheets of unidirectional graphite fibers embedded in Amoco's ERL1962 resin.

The unidirectional plies were laid up in (0°, 30°, 60°, 90°, 120°, 150°) orientations to achieve pseudo isotropic properties. Face sheets were 24-ply; ribs were 12-ply. A tin-indium moisture barrier was added to enhance long-term dimensional stability and prevent contamination of optical components.

The kinematic mounting system uses titanium ball mounts—one for each translational degree of freedom (1D, 2D, and 3D support). Titanium provides good thermal compatibility with the composite bench due to its low CTE and poor thermal conductivity.

---

## Optical Bench Requirements and FEM Analysis

The bench had to survive:

- Temperature extremes of  $-40^{\circ}\text{C}$  to  $+60^{\circ}\text{C}$ ,
- Quasi-static loads of  $-12.5 \text{ g} / +6.5 \text{ g}$  in the thrust direction (x),
- Loads of  $\pm 6.5 \text{ g}$  in lateral directions (y and z),
- Attachment constraints of  $\pm 35 \text{ g}$  normal,  $\pm 20 \text{ g}$  in-plane, and
- Lifting constraints of  $\pm 3 \text{ g}$  in the x-direction.

The system was required to have a minimum fundamental stiffness of 100 Hz to prevent coupling with other components, and a maximum mass of 6.8 kg.

To validate the system, an FEM was developed to:

- Simulate quasi-static load conditions,
- Evaluate distortions,
- Identify natural frequencies.

Final modal analysis revealed:

- 111 Hz: Bending in thrust direction (x),
- 138 Hz: Twisting of star camera mount plane,
- 203 Hz: Bending in lateral direction.

## Hazard Classification

Propellants are classified based on their hazard potential, especially whether they can transition from deflagration (rapid burning) to detonation (explosive shock).

- **Class 1.1** propellants are more hazardous and can detonate, causing complete and violent energy release.

- **Class 1.3** propellants typically burn without detonating, even if the motor case ruptures under pressure.

Tests such as **impact tests** and **card gap tests** are used to determine classification.

The classification affects **labeling, shipping regulations, storage limits, and safety distances**, as defined by the **U.S. Department of Defense (DOD)** and **United Nations standards**.

---

## Insensitive Munitions

Insensitive munitions are designed to minimize unintentional explosions and improve safety.

Typical insensitivity tests include:

- Fast cook-off (direct fire exposure)
- Slow cook-off (gradual heating)
- Bullet impact
- Fragment impact
- Sympathetic detonation (nearby explosion)
- Shaped charge impact
- Spall impact (fragments from steel plate)

Passing criteria: no detonation, and at most, contained burning.

If detonation occurs during testing, the motor must be redesigned or the propellant changed.

Recent insensitive propellants (e.g., HTPE-based and Butacene-based binders) offer reduced sensitivity to external stimuli like fire or impacts, and have been adopted in systems like the Evolved Sea Sparrow Missile (ESSM).

---

## Upper Pressure Limit

Propellants can detonate if the pressure becomes too high, especially during extreme conditions such as impact or gun-launch acceleration.

- Detonation pressures range from 300 MPa (45,000 psi) to 1500 MPa (225,000 psi) depending on the propellant type.

These limits define the safe operational boundary of the propellant.

---

## Toxicity

While many solid propellants are not highly toxic once cured, certain ingredients and intermediates can be hazardous:

- Crosslinking agents and catalysts may cause skin or respiratory irritation, or be carcinogenic.
  - Safety during production involves using gloves, face shields, ventilation, and sometimes gas masks.
  - Exhaust gases can be toxic, especially when beryllium, chlorine, or ammonium perchlorate are present, producing hydrochloric acid in the plume.
  - Facilities must follow strict decontamination and safety protocols.
- 

## Safety Rules

Effective safety management includes:

1. Training personnel on hazards and emergency responses.
2. Designing motors and equipment with safety in mind.
3. Enforcing strict safety protocols, such as:
  - No smoking near propellants
  - Use of spark-proof tools and footwear
  - Shielding electrical systems
  - Fire suppression (e.g., water deluge systems)
  - Proper grounding to avoid static discharge

These rules are essential in manufacturing, testing, and launch operations to prevent accidents.

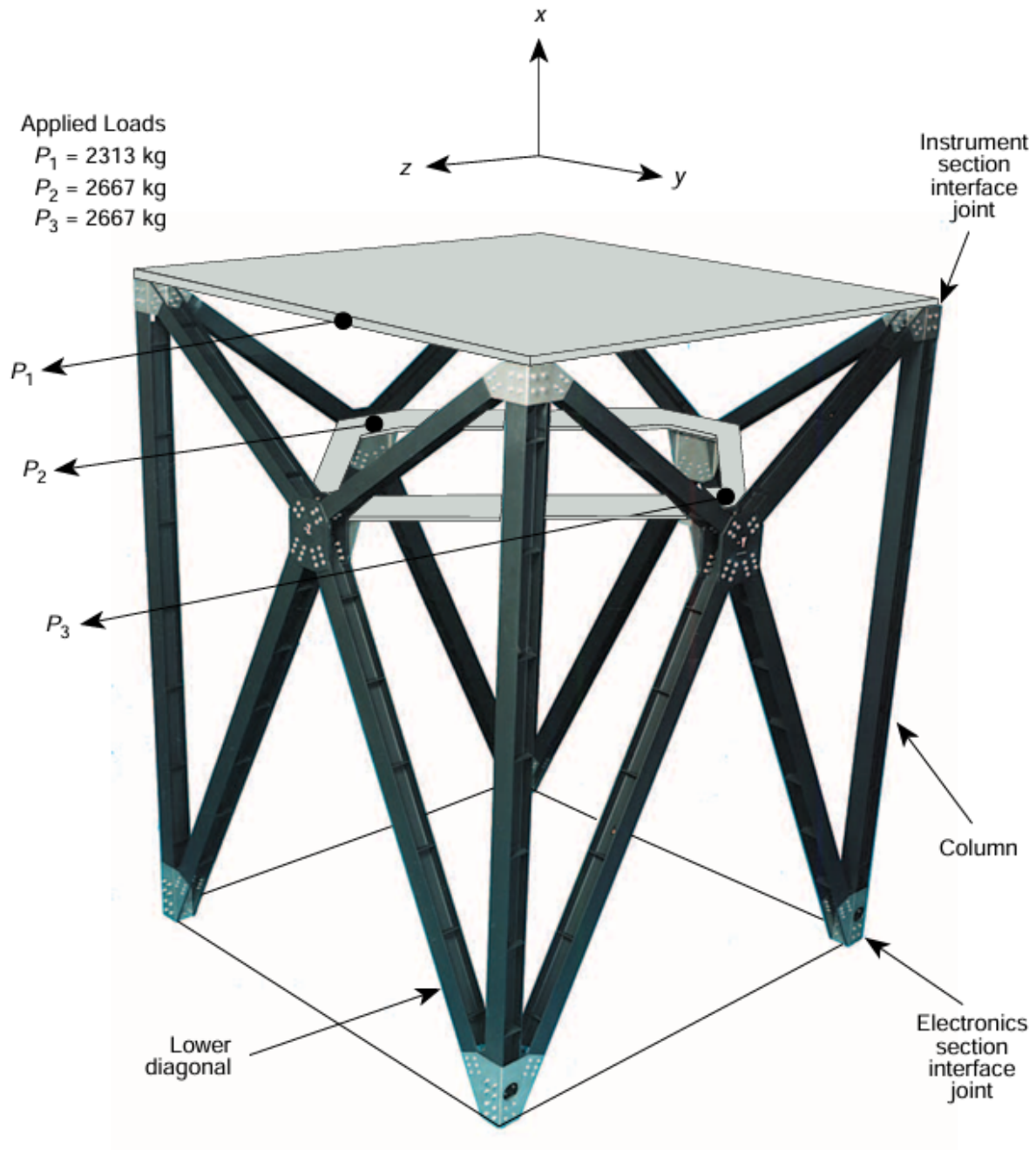


**Figure 12.** Truss structure static load test set-up.

**PROPELLANT INGREDIENTS**

A number of relatively common propellant ingredients are listed in Table

13-6 for double-base propellants and for composite-type solid propellants in Table 13-7.

TABLE 13-6. Typical Ingredients of Double-Base (DB) Propellants and Composite-Modified Double-Base (CMDB) Propellants  
a Several of these, but not all, are added to CMDB propellant.

Type	Percent	Acronym	Typical Chemicals
Binder usually plasticized with 20-50% nitroglycerine	30-50	NC	Nitrocellulose (solid),
Reactive plasticizer (liquid explosive)	20-50	NG DEGDN TEGDN PDN TMETN	Nitroglycerine Diethylene glycol dinitrate Triethylene glycol dinitrate Propanediol dinitrate Trimethylolethane trinitrate
Plasticizer (organic liquid fuel)	0-10	DEP TA DMP EC DBP	Diethyl phthalate Triacetin Dimethyl phthalate Dioctyl phthalate Dibutyl phthalate
Burn Rate Modifier	Up to 3	PbSa PbSt CuSa CuSt	Lead salicylate Lead stearate Copper salicylate Copper stearate
Coolant	>1	OXM	Oxamide
Opacifier graphite powder)	Up to 2	C	Carbon black (powder or
Stabilizer / Antioxidant	> 0.3	DED EC DPA	Diethyl diphenyl Ethyl centralite Diphenylamine
Visible Flame Suppressant	0-15	KNO <sub>3</sub> K <sub>2</sub> SO <sub>4</sub>	Potassium nitrate Potassium sulfate
Lubricant (extruded only)	0-15	C Al	Graphite Wax
Metal fuel a (solid)	0-20	Al	Aluminum, fine powder
Crystalline oxidizer a	-	AP AN	Ammonium perchlorate Ammonium nitrate
Solid explosive crystals a Cyclotetramethylenetrinitramine	-	HMX RDX NQ	Cyclotrimethylenetrinitramine Nitroguanidine

TABLE 13-7. Typical Ingredients of Composite Solid Propellants

Type	Percent	Acronym	Typical Chemicals
Oxidizer (crystalline)	0-70	AP AN KP KN ADN	Ammonium perchlorate Ammonium nitrate Potassium perchlorate Potassium nitrate Ammonium dinitramide
Metal fuel	0-30	Al Be Zr	Aluminum Beryllium (experimental only) Zirconium (also burn rate modifier)
Fuel/Binder (polybutadiene)	5-18	HTPB	Hydroxyl-terminated
polybutadiene		CTPB	Carboxyl-terminated
polybutadiene		PBAN PBAA	Polybutadiene acrylonitrile Polybutadiene acrylic acid
Fuel/Binder (polyether/polyester)	0-15	PEG PCP PGA PPG HTPE	Polyethylene glycol Polycaprolactone polyol Polyglycol adipate Polypropylene glycol Hydroxyl-terminated
polyether		PU	Polyurethane
Curing Agent / Crosslinker	0.2-3.5	IPDI TDI DDI TMP BITA	Isophorone diisocyanate Toluene-2,4-diisocyanate Dimethyl diisocyanate Trimethylol propane
Trimesoyl-1(2-ethyl)-aziridine			
Burn Rate Modifier	0.2-3	FeO nBF (Various)	Ferric oxide n-Butyl ferrocene Oxides of Cu, Pb, Zr, Fe
Explosive Filler (solid)	0-40	HMX	
Cyclotetramethylenetrinitramine		RDX	
Cyclotrimethylenetrinitramine		NQ CL-20	Nitroguanidine
Hexanitrohexaazaisowurtzitane			
Plasticizer / Pot Life Ctrl	0-7	DOP DOA DOS DMP	Diethyl phthalate Diethyl adipate Diethyl sebacate Dimethyl phthalate

<b>Energetic Plasticizer</b>	0-14	IDP GAP NG DEGDN BTTN TEGDN TMETN PCP	Isodecyl pelargonate Glycidyl azide polymer Nitroglycerine Diethylene glycol dinitrate Butanetriol trinitrate Triethylene glycol dinitrate Trimethylolethane trinitrate Polycaprolactone polymer
------------------------------	------	--	---

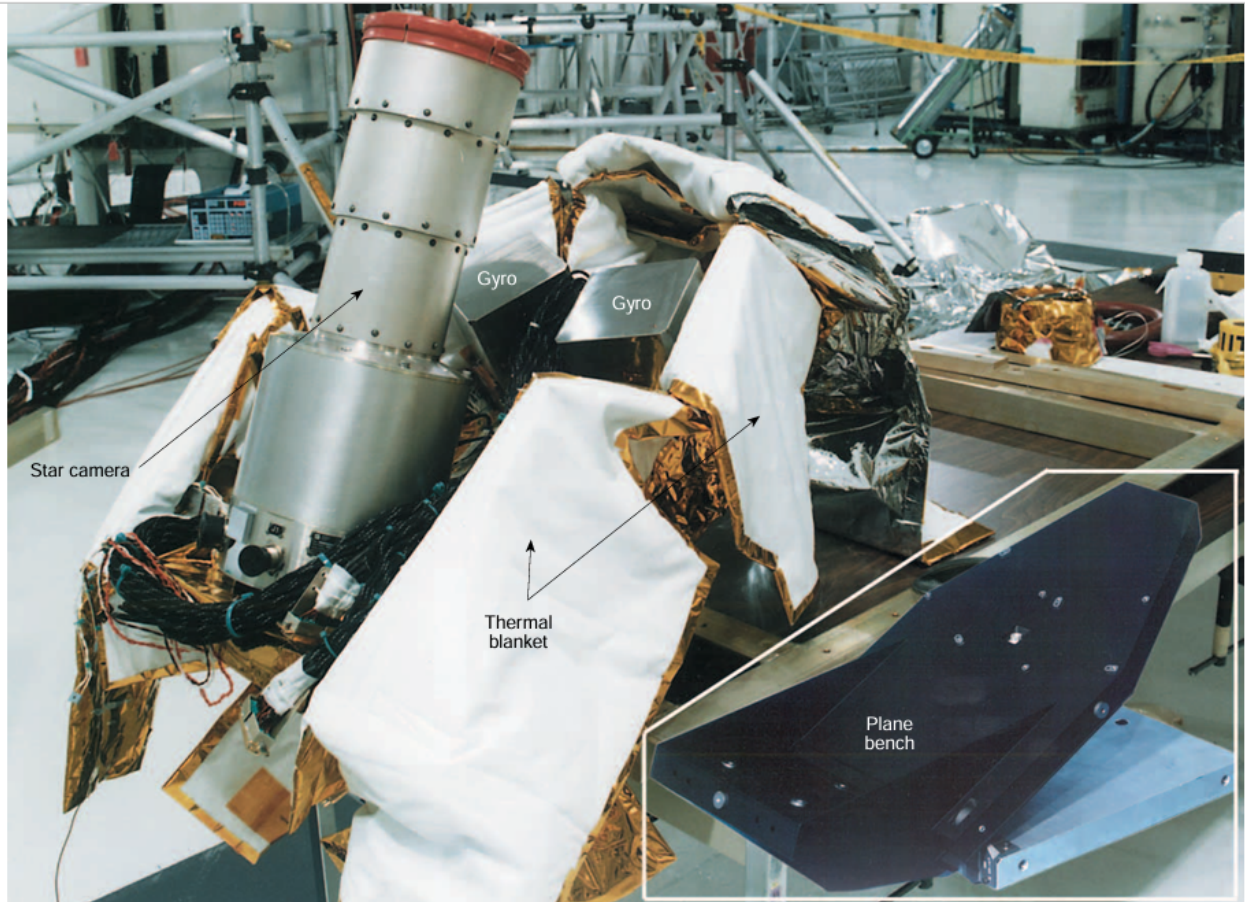


Figure 13. MSX optical bench (structure shown in lower right).

#### Fiber Reinforcement

Table 2.15 Brand names and properties of ultra-high-modulus (uhm) carbon fibers:

P100Sa: Young's modulus = 724 GPa, Tensile strength = 2.20 GPa, Tensile strain = 0.31 %, Thermal conductivity = -1.45 W/(mK), Coefficient of

thermal expansion =  $520 \times 10^{-6} \text{ K}^{-1}$ , Electrical conductivity =  $2.5 \text{ } \Omega\text{-cm}$ , Density =  $2.15 \text{ g/cm}^3$ .

P120Sa: Young's modulus = 827 GPa, Tensile strength = 2.20 GPa, Tensile strain = 0.27 %, Thermal conductivity =  $-1.45 \text{ W/(mK)}$ , Coefficient of thermal expansion =  $640 \times 10^{-6} \text{ K}^{-1}$ , Electrical conductivity =  $2.2 \text{ } \Omega\text{-cm}$ , Density =  $2.18 \text{ g/cm}^3$ .

M60J: Young's modulus = 588 GPa, Tensile strength = 3.92 GPa, Tensile strain = 0.70 %, Thermal conductivity =  $-0.90 \text{ W/(mK)}$ , Coefficient of thermal expansion =  $75 \times 10^{-6} \text{ K}^{-1}$ , Electrical conductivity =  $8.0 \text{ } \Omega\text{-cm}$ , Density =  $1.94 \text{ g/cm}^3$ .

M70J: Young's modulus = 690 GPa, Tensile strength = -, Tensile strain = -, Thermal conductivity = -, Coefficient of thermal expansion = -, Electrical conductivity = -, Density = -.

Gy-70: Young's modulus = 517 GPa, Tensile strength = 1.86 GPa, Tensile strain = 0.36 %, Thermal conductivity =  $-1.10 \text{ W/(mK)}$ , Coefficient of thermal expansion =  $142 \times 10^{-6} \text{ K}^{-1}$ , Electrical conductivity =  $6.5 \text{ } \Omega\text{-cm}$ , Density =  $1.90 \text{ g/cm}^3$ .

Gy-80: Young's modulus = 527 GPa, Tensile strength = 1.96 GPa, Tensile strain = 0.32 %, Thermal conductivity = -, Coefficient of thermal expansion =  $6.0 \times 10^{-6} \text{ K}^{-1}$ , Electrical conductivity = -, Density =  $1.92 \text{ g/cm}^3$ .

(Note: aPitch-based carbon fibers)

---

Table 2.16 Brand names and properties of Chinese PAN-based carbon fibers:

J9107 (Jilin Carbon Co. Ltd.): Tensile strength = 3.49 GPa, Young's modulus = 227.6 GPa, Tensile strain = 1.63 %, Density =  $1.68 \text{ g/cm}^3$ , Diameter =  $6.3 \mu\text{m}$ , Electrical conductivity =  $19.6 \times 10^{-6} \text{ } \Omega\text{-cm}$ .

S9206 (Shanghai Carbon Co. Ltd.a): Tensile strength = 3.10 GPa, Young's modulus = 217.3 GPa, Tensile strain = 1.45 %, Density =  $1.71 \text{ g/cm}^3$ , Diameter =  $6.3 \mu\text{m}$ , Electrical conductivity =  $19.8 \times 10^{-6} \text{ } \Omega\text{-cm}$ .

L8506 (Lanzhou Carbon Co. Ltd.a): Tensile strength = 2.90 GPa, Young's modulus = 203.3 GPa, Tensile strain = 1.48 %, Density =  $1.71 \text{ g/cm}^3$ , Diameter =  $6.5 \mu\text{m}$ , Electrical conductivity =  $24.8 \times 10^{-6} \text{ } \Omega\text{-cm}$ .

## Pitch-Based Carbon Fibers

As raw materials; bituminous coal, petroleum bitumen and asphalt or polyoxyethylene asphalt should be appropriately treated so that their rheological property, chemical composition and structure will meet the requirements for carbonization and graphitization. Asphalt can be isotropic or anisotropic (such as mesopitch or LCD).

**Carbon fibers** derived from the isotropic system generally have poor performance; for example, their tensile strength is about 950 MPa, Young's modulus is 40–45 GPa and the tensile strain is 2.0–2.2%. These fibers are referred to as common-class products and are mainly used in composites that do not require high performance. Alternatively, high-performance carbon fibers, particularly the ultra-high-modulus carbon fibers can be manufactured from mesopitch.

Since the original carbon content of pitch is higher than that of PAN, its carbon yield is higher after carbonation. In addition to a high Young's modulus, pitch-based carbon fibers also have good thermal conductivity, electrical conductivity and a negative coefficient of thermal expansion. However, their processing properties and compressive strength are not as good as those of PAN-based carbon fibers.

High-performance pitch-based carbon fibers have unique applications in aerospace and space satellites, etc. The mechanical properties of some typical commercial pitch-based carbon fibers are listed below:

### **Amoco Corp.**

- Thornel P25: Tensile strength = 1.40 GPa, Young's modulus = 140 GPa, Tensile strain = 1.0%
- Thornel P55: Tensile strength = 2.10 GPa, Young's modulus = 380 GPa, Tensile strain = 0.5%
- Thornel P75: Tensile strength = 2.00 GPa, Young's modulus = 500 GPa, Tensile strain = 0.44%
- Thornel P100: Tensile strength = 2.20 GPa, Young's modulus = 690 GPa, Tensile strain = 0.30%
- Thornel P120: Tensile strength = 2.20 GPa, Young's modulus = 820 GPa, Tensile strain = 0.20%

## Danncarl

- F140: Tensile strength = 1.80 GPa, Young's modulus = 140 GPa, Tensile strain = 1.3%
- F60: Tensile strength = 3.00 GPa, Young's modulus = 600 GPa, Tensile strain = 0.5%

## Kureca

- KCF100: Tensile strength = 0.90 GPa, Young's modulus = 38 GPa, Tensile strain = 2.4%
- KCF200: Tensile strength = 0.85 GPa, Young's modulus = 42 GPa, Tensile strain = 2.1%

The Granoc XN series are low modulus, low strength carbon fibers with a fiber diameter of about 10  $\mu\text{m}$ , Young's modulus of 55–155 GPa, tensile strength of 1.10–2.40 GPa, low density (1.65–2.80 g/cm<sup>3</sup>), and tensile strain of 1.5–2.0%. Mainly used in civil engineering and infrastructure as sealing materials, reinforcing sheets for repairing concrete, tunnel walls, and poles.

The Granoc CN series are carbon fibers mainly used for recreational sport supplies and general industrial applications.

Compared with T300-type PAN-based carbon fibers, their Young's modulus is much higher and suitable for materials

requiring stiffness. Applications include electronic equipment, precision optical instruments, acoustics, audio equipment, robot arms, and various rollers.

The Granoc YSH series of carbon fibers are mainly used in manufacturing satellite antennas, satellite structure components,

solar panels, joysticks, strings, missile components, and rocket components.

In China, research focuses on common pitch-based carbon fibers using isotropic pitch as the precursor and high-performance

pitch-based carbon fibers using mesopitch as the precursor. Common carbon fibers have tensile strength 0.80–0.95 GPa, Young's

modulus 40–45 GPa, tensile strain 2.0–2.5%, but are not industrialized yet. Due to poor mechanical properties, they are mainly used for functional or cement matrix composites.

High-performance pitch-based carbon fibers are prepared from mesopitch by melt spinning, pre-oxidation, carbonation, and graphitization.

Performance largely depends on precursor structure and composition. Mesopitch studies led to graphite fibers produced by modification

of oil residue and coal. Spinnable pitch softening point is 264–278 °C with mesopitch content above 95%. Typical mechanical properties

of final continuous carbon fibers are listed below.

## COMPONENTS

### Nippon Graphite Fiber Corporation carbon fibers:

- XN-05: Tensile strength = 1.10 GPa, Young's modulus = 54 GPa, Tensile strain = 2.0%, Density = 1.65 g/cm<sup>3</sup>, Diameter = 10 μm,

Coefficient of thermal expansion =  $+3.4 \times 10^{-6}$  K<sup>-1</sup>, Thermal conductivity = 47 W/(mK), Electrical conductivity =  $28 \times 10^{-4}$  Ωcm

- XN-10: Tensile strength = 1.70 GPa, Young's modulus = 110 GPa, Tensile strain = 1.6%, Density = 1.70 g/cm<sup>3</sup>, Diameter = 10 μm,

Coefficient of thermal expansion =  $-0.1 \times 10^{-6}$  K<sup>-1</sup>, Thermal conductivity = –, Electrical conductivity =  $100 \times 10^{-4}$  Ωcm

- XN-15: Tensile strength = 2.40 GPa, Young's modulus = 155 GPa, Tensile strain = 1.5%, Density = 1.85 g/cm<sup>3</sup>, Diameter = 10 μm,

Coefficient of thermal expansion =  $-0.8 \times 10^{-6}$  K<sup>-1</sup>, Thermal conductivity = 6.3 W/(mK), Electrical conductivity =  $20 \times 10^{-4}$  Ωcm

- CN-05: Tensile strength = 3.43 GPa, Young's modulus = 620 GPa, Tensile strain = 0.6%, Density = 2.12 g/cm<sup>3</sup>

- CN-15: Tensile strength = 3.43 GPa, Young's modulus = 780 GPa, Tensile strain = 0.5%, Density = 2.17 g/cm<sup>3</sup>

- YSH-50A10H: Tensile strength = 3.83 GPa, Young's modulus = 520 GPa, Tensile strain = 0.7%, Density = 2.10 g/cm<sup>3</sup>, Diameter = 6 μm,

Coefficient of thermal expansion =  $-1.4 \times 10^{-6}$  K<sup>-1</sup>, Thermal conductivity = 140 W/(mK), Electrical conductivity =  $7 \times 10^{-4}$  Ωcm

- YSH-50A15S: Same as above except Diameter = 7  $\mu\text{m}$
- YSH-60A: Tensile strength = 3.83 GPa, Young's modulus = 630 GPa, Tensile strain = 0.6%, Density = 2.12 g/cm<sup>3</sup>, Diameter = 7  $\mu\text{m}$ ,
 

Coefficient of thermal expansion =  $-1.4 \times 10^{-6} \text{ K}^{-1}$ , Thermal conductivity = 200 W/(mK), Electrical conductivity =  $6 \times 10^{-4} \Omega\text{cm}$
- YSH-70A: Tensile strength = 3.83 GPa, Young's modulus = 720 GPa, Tensile strain = 0.5%, Density = 2.15 g/cm<sup>3</sup>, Diameter = 7  $\mu\text{m}$ ,
 

Coefficient of thermal expansion =  $-1.5 \times 10^{-6} \text{ K}^{-1}$ , Thermal conductivity = 260 W/(mK), Electrical conductivity =  $5 \times 10^{-4} \Omega\text{cm}$
- YS-80A: Tensile strength = 3.63 GPa, Young's modulus = 785 GPa, Tensile strain = 0.5%, Density = 2.15 g/cm<sup>3</sup>, Diameter = 7  $\mu\text{m}$ ,
 

Coefficient of thermal expansion =  $-1.5 \times 10^{-6} \text{ K}^{-1}$ , Thermal conductivity = 320 W/(mK), Electrical conductivity =  $5 \times 10^{-4} \Omega\text{cm}$
- YS-90A: Tensile strength = 3.53 GPa, Young's modulus = 880 GPa, Tensile strain = 0.3%, Density = 2.18 g/cm<sup>3</sup>, Diameter = 7  $\mu\text{m}$ ,
 

Coefficient of thermal expansion =  $-1.5 \times 10^{-6} \text{ K}^{-1}$ , Thermal conductivity = 500 W/(mK), Electrical conductivity =  $3 \times 10^{-4} \Omega\text{cm}$
- YS-95A: Tensile strength = 3.53 GPa, Young's modulus = 920 GPa, Tensile strain = 0.3%, Density = 2.19 g/cm<sup>3</sup>, Diameter = 7  $\mu\text{m}$ ,
 

Coefficient of thermal expansion =  $-1.5 \times 10^{-6} \text{ K}^{-1}$ , Thermal conductivity = 660 W/(mK), Electrical conductivity =  $2.2 \times 10^{-4} \Omega\text{cm}$

## STRUCTURE

**Gusset plates** were constructed from multiple layers of unidirectional tape oriented in a (0°, 30°, 60°, 90°, 120°, 150°) \_S\_N lay-up to yield a pseudo isotropic condition. The core ribs were 12-ply, and the face sheets were 24-ply laminates. Material properties for this configuration are given in Table 5. A tin-indium moisture barrier similar to that used on the truss was applied to prevent moisture effects on the stability of the optical bench. This barrier also helps minimize moisture contamination of the sensor optics located on the forward part of the structure.

The configuration for the kinematic mount system uses a ball mount concept that provides nonredundant translational support in one, two, and three directions for the three mounts. The mounts attach to the optical bench at the central plane of the bench thickness. This attachment method limits moment transfer between the spacecraft and the optical bench, minimizing distortion of the mounted structure. The mounts

were made from titanium to provide good thermal compatibility (low coefficient of thermal expansion, CTE) with the composite bench; additionally, titanium is a relatively poor conductor, providing thermal isolation between the bench and the instrument section.

The optical bench structure must meet all requirements after exposure to temperature extremes of -240°C and +60°C. Quasistatic load strength requirements of 212.5 g / +6.5 g in the spacecraft thrust direction (x), and  $\pm 6.5$  g in the spacecraft lateral directions (y and z), were imposed to ensure the hardware survives the launch environment. Additional load constraints were placed on component attachments ( $\pm 35$  g normal and  $\pm 20$  g parallel to the component's mounting plane) and lifting attachments ( $\pm 3$  g in the lift direction [x]) to guarantee attachment integrity. A stiffness requirement of 100 Hz was desired to prevent dynamic interactions with other structural components. Given all these requirements, the system's mass was limited to not exceed 6.8 kg.

To predict the optical bench system's capability, a finite element model (FEM) was generated to examine quasistatic loading conditions, determine fundamental dynamic characteristics, and evaluate bench distortions. After examining numerous concepts and iterating to the final version, the fundamental dynamic characteristics were determined to be: 111 Hz (bench bending in the thrust direction), 138 Hz (twisting of the star camera mounting plane), and 203 Hz (bench bending in the lateral direction). Results of the quasistatic loading analysis indicated that, in general, except for certain local areas, the structural design exhibits ample structural margins under the given conditions. For components such as the optical bench, which are driven by stiffness requirements, moderate stress levels from mechanical loads are typical. A summary of the minimum safety margins for each bench structural component is presented in Table 6.

To determine compliance with alignment and stability requirements, a thermal distortion analysis for operational conditions was performed using the FEM. This included thermal gradient conditions as well as the effects of the breakaway torque of the kinematic mounts. The results indicate a maximum relative displacement of 0.00635 mm and a maximum relative distortion of 1.35 arcseconds under operating conditions. This maximum occurs between the star camera and autocollimators. For each inch-pound of breakaway torque, an additional 0.1 arcseconds of rotational deformation occurs. To minimize this impact, bearings with breakaway torques not exceeding 0.17 kg·m were selected. The total anticipated distortion for this configuration is thus 1.65 arcseconds. Breakaway torque has a negligible impact on displacement.

<b>Property</b>	<b>Value</b>
Tensile strength ( $0^\circ$ )	$2.951 \times 10^8$ N/m <sup>2</sup>
Tensile modulus ( $0^\circ/90^\circ$ )	$1.05 / 1.03 \times 10^{11}$ N/m <sup>2</sup>
Tensile Poisson ratio ( $0^\circ/90^\circ$ )	0.32 / 0.32
Compression strength ( $0^\circ/90^\circ$ )	$1.68 / 1.78 \times 10^8$ N/m <sup>2</sup>

Compression modulus (0°/90°)	0.95 / 1.04 × 10 <sup>11</sup> N/m <sup>2</sup>
Compression Poisson ratio (0°/90°)	0.32 / 0.32
Flatwise tensile	1.17 × 10 <sup>7</sup> N/m <sup>2</sup>
In-plane shear strength	1.81 × 10 <sup>8</sup> N/m <sup>2</sup>
Coefficient of Thermal Expansion (0°/90°)	20.22 × 10 <sup>-6</sup> in/in/°C